UNIVERSITÀ DEGLI STUDI DI PADOVA

SCUOLA DI SCIENZE

Dipartimento di Geoscienze

Direttore Prof. Nicola Surian

TESI DI LAUREA MAGISTRALE IN

GEOLOGIA E GEOLOGIA TECNICA

MORPHOMETRIC ANALYSIS OF LAVA TUBES

Relatore: Prof. Matteo Massironi

Correlatore: Dott. Francesco Sauro

Correlatore: Dott. Riccardo Pozzobon

Laureando: Alessandro Marraffa

Matricola: 2017363

ANNO ACCADEMICO 2023-2024

Contents

Abstract

Lava tubes (also known as pyroducts) are objects of great interest not only for their role in the formation of lava flow fields on Earth, but also for their implications on the emplacement of lava terrains across the Solar System. These features have been detected on the surface of Mars and the Moon through satellite imagery as sinuous collapse chains interpreted as the surface evidence of subsurface conduits. For this reason, volcano-speleogenetic processes on Earth can be used as analogues of similar subsurface features on different planetary bodies. Indeed, since to date subsurface conduits has not been observed yet, through the study of terrestrial analogues it is possible to infer the potential lava tube morphologies beneath the surface of Mars and the Moon. Several maps and surveys of lava tubes, collected in regional caving records around the world, show a wide variety of lava tube morphologies. Different authors have proposed possible morphometrics indices to describe the genetic features of some particular karst caves. Here, we have applied the same approach to terrestrial lava tubes. Digitizing and collecting lava tube surveys in several sites all over the world allowed us to extract several dimensional parameters and develop a global database. An initial observation of the surveys was necessary to understand qualitative morphological differences, and then morphometric indices were extracted, to recognize, through a statistical approach, a quantitative relationship between lava tubes morphologies and their genetic processes, in different volcanic settings. Indeed, lava tubes on Earth have different morphologies and a huge difference in size, potentially associated with specific eruptive (effusion rates, trend and duration of the eruption) and slope parameters. In this work we analyze and discuss this variability, trying to extrapolate useful information to understand lava tube genetic processes even on other planetary bodies.

Riassunto

I tubi di lava (noti anche come *"pyroduct"*) sono oggetto di grande interesse, non solo per il loro ruolo nella formazione dei campi lavici sulla Terra, ma anche per le loro implicazioni sulla formazione dei terreni lavici in tutto il Sistema Solare. Queste morfologie sono state rilevate sulla superficie di Marte e della Luna, le immagini satellitari hanno evidenziato lunghe catene sinuose formate da morfologie di collasso, queste sono state interpretate come l'evidenza superficiale di gallerie ipogee. I processi vulcano-speleogenetici che danno luogo a simili morfologie sulla Terra, possono essere utilizzati come analoghi delle possibili morfologie del sottosuolo sui diversi corpi planetari. Infatti, poiché ad oggi non sono ancora stati osservati direttamente i condotti ipogei (tubi di lava), attraverso lo studio degli analoghi terrestri è possibile dedurre le potenziali morfologie dei tubi di lava sotto la superficie di Marte e della Luna. Gli archivi speleologici regionali di tutto il mondo raccolgono una grande quantità di mappe e rilievi di tubi di lava, i quali mostrano un'ampia varietà di morfologie e caratteristiche. Diversi autori hanno proposto vari indici morfometrici per descrivere le caratteristiche genetiche di alcune particolari grotte carsiche. Qui abbiamo applicato lo stesso approccio per i tubi di lava terrestri. La digitalizzazione e la raccolta di rilievi di tubi di lava in diversi siti di tutto il mondo ci ha permesso di estrarre diversi parametri dimensionali e di sviluppare un database globale. Un'osservazione iniziale dei rilievi è stata necessaria per comprendere le differenze morfologiche qualitative, in seguito sono stati estratti indici morfometrici utili per riconoscere, attraverso un approccio statistico, una relazione quantitativa tra le morfologie dei tubi di lava e i loro processi genetici, in diversi contesti vulcanici. Infatti, i tubi di lava sulla Terra hanno morfologie diverse e un'enorme differenza per dimensioni e morfologie, potenzialmente associate a specifici parametri eruttivi (tassi di effusione, andamento e durata dell'eruzione) e di pendenza. In questo lavoro analizziamo e discutiamo questa variabilità morfologica e di dimensioni, cercando di estrapolare informazioni utili per comprendere i processi genetici dei tubi di lava utili anche per altri corpi planetari.

1. Introduction

Lava tubes, also known as pyroducts, are a primary volcanic rock caves (Kempe, 2012; 2019), are defined as a "roofed conduit of flowing lava, either active, drained, or plugged" (Halliday, 2004; Sauro et al, 2020). Lava tubes is a hotly debated topic nowadays, given the important role of these structure in understanding the formation of lava terrains in the solar system, and their usefulness as analogs of potential subsurface morphologies on Mars and the Moon. During effusive volcanic eruptions, lava tubes work as thermally efficient conduits, where the minimization of heat loss allows the transport of lava flows over long distances up to several tens of kilometers (Tomasi et al., 2022). Indeed, the lengths of lava tubes on Earth vary from a few meters up to tens of kilometers (Bunnell, 2008). Their width and height vary from 0.5 m up to 30 m, from a few centimeters -below the surface to a depth of a few tens of meters (Sauro et al., 2020). Lava tubes can have several different patterns: single tubes, sinuous or rectilinear; braided tubes, with bifurcations and conjunctions; multilevel tubes with different levels connected by lava falls and shafts, or a combination of braided tubes on different levels (Sauro et al., 2020). This range of morphologic variability is due to different genetic processes controlled mainly by the effusion rate, the slope of the underlying substratum on which the lava flows, and the related rheology of the lava (Sauro et al., 2020).

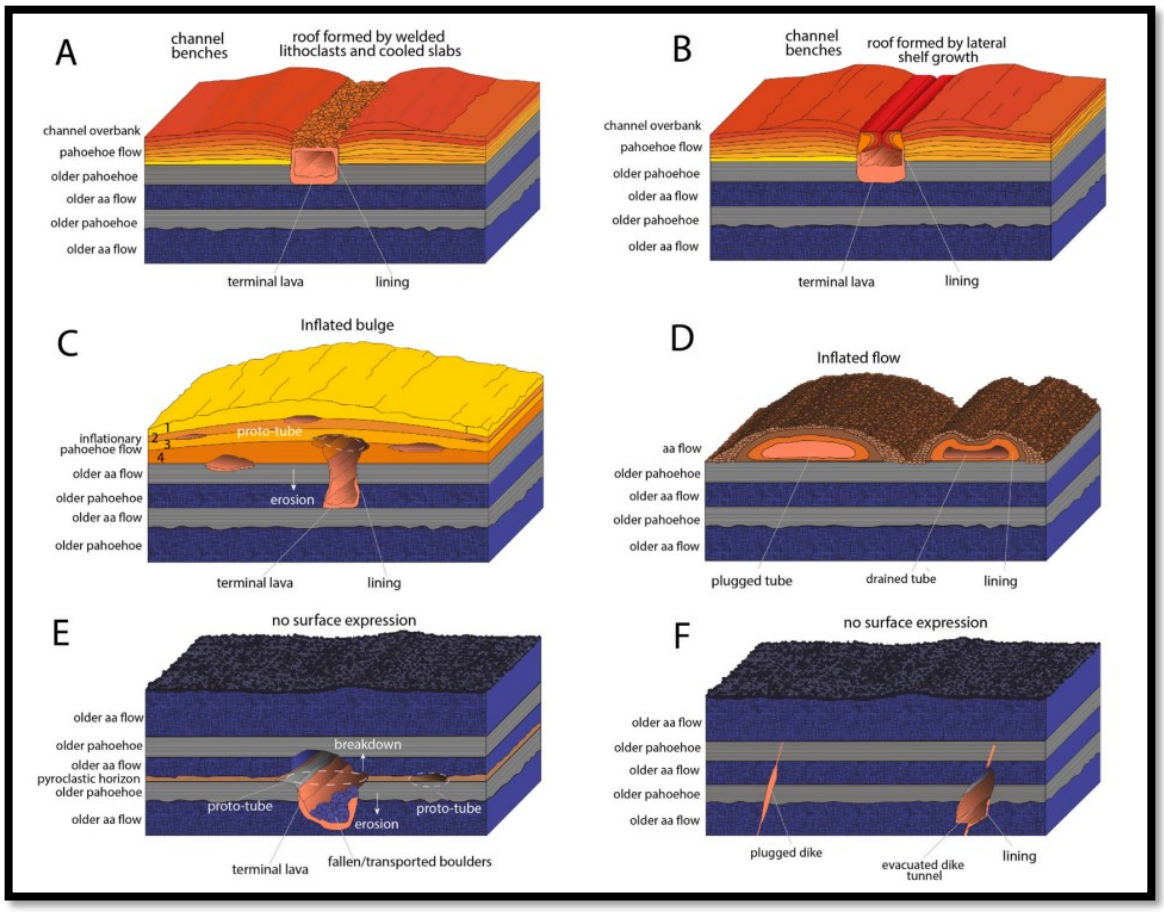

Figure 1: Spleogenetics processes of lava tube and their related morphologies. A-B) Lava tube formed by the overcrusting of channels by floating solidified slabs and lithoclasts welded together, lava tube within a channel formed by lateral shelf accretion and consecutive closure; C-D) Lava tube formed by shallow inflation of pahoehoe sheets and later downward erosion lava tube formed by inflation and draining of an aa flow nucleus; E-D) Lava tube formed by deep inflation along pre-existing lava flows boundaries or intra-flow pyroclastic deposits (inception horizons) enlarged by thermal erosion and breakdown tube formed through draining of a conduit formed by thermal erosion along a sealed fracture (eruptive fissure) (Sauro et al., 2020).

The main genetic process proposed was by "crusting over of a channel" (Francis, 1993), or "roofed conduit of flowing lava" (Halliday, 2004). The *"Overcrusting"* tube formation was observed for the first time during the long-lasting effusive eruptions at Kīlauea volcano in Hawaii by Peterson and Swanson (1974), and Peterson et al. (1994). This process is related to the principle that the outer surface of an active lava flow chills quickly

because of the temperature difference between the molten lava and the atmospheric air. The cooling surface becomes progressively more viscous and finally solidifies (Dragoni et al., 1995), insulating the molten lava below. Afterwards the insulation, slows the rate of cooling inside the closed tube helping to maintain heat and low viscosity over long distances and time, (Sauro et al., 2020). A different mechanism of formation, which is shallow inflation, initially acts within thin sheets of pahoehoe lava (Sauro et al, 2020). This sheet cools quickly, entrapping gases as vesicles that diminish it's overall density. Consequently, the sheet will float on top of the next pulse of advancing melt (the lava flow is "inflated" from below because of buoyancy) before forming the next distal surface sheet (Kempe, 2012; 2019). Multiple advances can occur, forming a primary roof composed of several sheets, separated by sheer interfaces (Kempe, 2012). Inflation is classically associated with pahoehoe flows, but it has documented also aa flow. The magnitude of the inflation strongly depends on effusion rates (Calvari and Pinkerton, 1999; Jones et al., 2018; Kempe, 2019). Lava tubes formed by shallow inflation are usually characterized by a superficial bulge (due to the inflation) along its development, and by an original horizontal elliptical cross-section although they can be entrenched by thermos-mechanical erosion (Sauro et al., 2020). In addition, to the "*overcrusted"* and shallowly inflated lava tube morphotypes, few cases on Earth have been proposed as "deep inflated-entrenched" lava tubes (Sauro et al., 2020). These formed through inflation along deep inception horizons following previous lava flow boundaries where, after inflation, the conduit has been enlarged by downward thermos-mechanical erosion and breakdown phenomena (Tonello, 2017; Kempe, 2019; Tomasi et al. 2022). Shallow inflation caves are characterized by roofs built of one or several sheets, sometimes more than ten (Kempe, 2012; 2019), while for deep-inflation tubes, layers of older lava flow are found above the caves roof. This roof structure can be studied at roof openings, called *pukas*, in Hawai'i (Kempe, 2012). If the collapse occurs after the flow terminated, is termed of cold puka, instead, if the flow is still active, are called hot *pukas* which serve as temporary rootless vents when the tunnel below is obstructed or even closed entirely. Lava erupting from these pukas can form rapidly cooling, thin, ropy pahoehoe, reinforcing the primary roofs, (Kempe, 2012). *Pukas*, cold or hot, can also serve as entrances for the lava of later flows (Kempe, 2012). The name Pukas is used only for Hawaiian and Galapagos lava tubes, the lava tube entrances are also called skylights when

they form during lava flow (i.e., Hot Pukas) and collapse, (i.e., Cold Pukas) or more in general Jameo in Canary Island. (Sauro et al., 2020; Tomasi et al., 2022). Different genetic processes mean several variations in cave morphology: dimension, total depth, plane length, and many other parameters, can differ from one tube to another. These morphological parameters can quantitatively describe the lava tubes. Thanks to a 2-D survey Piccini (2011), obtained many morphometric indices used to describe karst caves, with different patterns and parameters. Thanks to a huge amount of data taken by cavers all around the world, nowadays we have many dates about karst, pseudo-karst, and volcanic caves. All the available data were taken by cavers using a cave compass (Suunto type), a clinometer, and a tape meter or, more recently, a laser meter. The use of laser meters allows easy and quick measuring of cross sections of conduits at each survey station. Compass or laser meters are not always usable for lava tube surveys, as these can be particularly susceptible to the presence of ferrous materials (iron minerals within basalts such as: Hematite, Ilmenite, Magnetite, Olivine). Theodolite is used to measure the direction of the tube. 2-D survey of a cave is not an easy task and the results depend on who made the survey and how deep it goes. Such parameters are not usually described in cave inventories, so this kind of analysis requires a specific elaboration of the cave surveys (Piccini, 2011). The amount of data available to be extracted from 2-D surveys can be useful to distinguish the different types of caves, in a relationship to a different genetic process. Therefore, a similar approach was used in this work, to extract parameters and indices, to characterize and better understand the lava tubes and their evolution, thanks to a quantitative perspective. For this goal, I digitized 36 lava tube surveys around the world which show great variety in morphology and size. These were collected from five different places, which show some similarities from a tectonic-volcanic point of view. The dimensional parameters and indices extracted from the lava tube surveys were compared with each other by plotting them on scatter plots. This made it possible to observe some correlations between parameters and indices, which are useful for understanding spelogenesis and lava tube evolution.

2-Geological settings:

In this chapter, I will introduce the different sites where the lava tubes considered in this study are located.

2.1-Mount Etna (Sicily)

Mount Etna is on the Eastern side of Sicily Island and, more specifically, on the suture between the converging European and African plates, adjacent to the subduction-related Aeolian Island arc (Schiano, 2001). However, there is no clear evidence that this volcanism is directly connected with active subduction beneath the Aeolian arc; there is no subduction-related seismic trace beneath Sicily (Schiano 2001).

Mount Etna covers an area of 1,190 km2, with a basal circumference of 140 km. This volcano with an elevation of 3,357 m (a.s.l.), is the tallest in Europe. volcanism at Mount Etna is composed for the most of intermediate alkaline lavas (Schiano, 2001). Branca's (2011) work on Etna suggests a comprehensive history of Etna's volcanism. Thanks to radio-isotopic dating $^{40}Ar/^{39}Ar$ from De Beni (2011), was indeed possible to define the stratigraphic setting in the new geological map (image 1), which is based on the combination of three different categories of stratigraphic units (Branca, 2011).

The main phases of the eruptive activity according to the proposed supersynthems classification are: (Branca, 2011).

1. Basalt Tholeiitic Supersynthems.
2. Timpe Supersynthems.
3. Valle del Bove Supersynthems.
4. Stratovolcano Supersynthems.

The oldest basalt tholeiitic unit is the product of a long period of scattered fissure-type eruptions, distributed first in the Pleistocene foredeep basin about 500 ka, which outcrops south of Mt. Etna and locally along the Ionian shoreline, at the front of the Sicilian fold and thrust belt, then from about 330 ka ago in a subaerial environment, (Branca, 2011; Barreca et al. 2018). The Timpe Supersynthem marks a significant change in the eruptive history of the Etna region around 220 ka, when Na-alkaline magma started rising more efficiently from the mantle. During the third phase, named Valle del Bove, the shifting of the magma source in the Valle del Bove area and the beginning of the central-type

volcanism occurred with the formation of several small polygenic volcanic centers that were active between at least 110 ka and 60 ka (De Beni et al., 2011; Branca and Ferrara, 2013). The final Stratovolcano Supersynthem marks the definitive stabilization in the present position of Etna's plumbing system from about 57 ka (Branca, 2011).

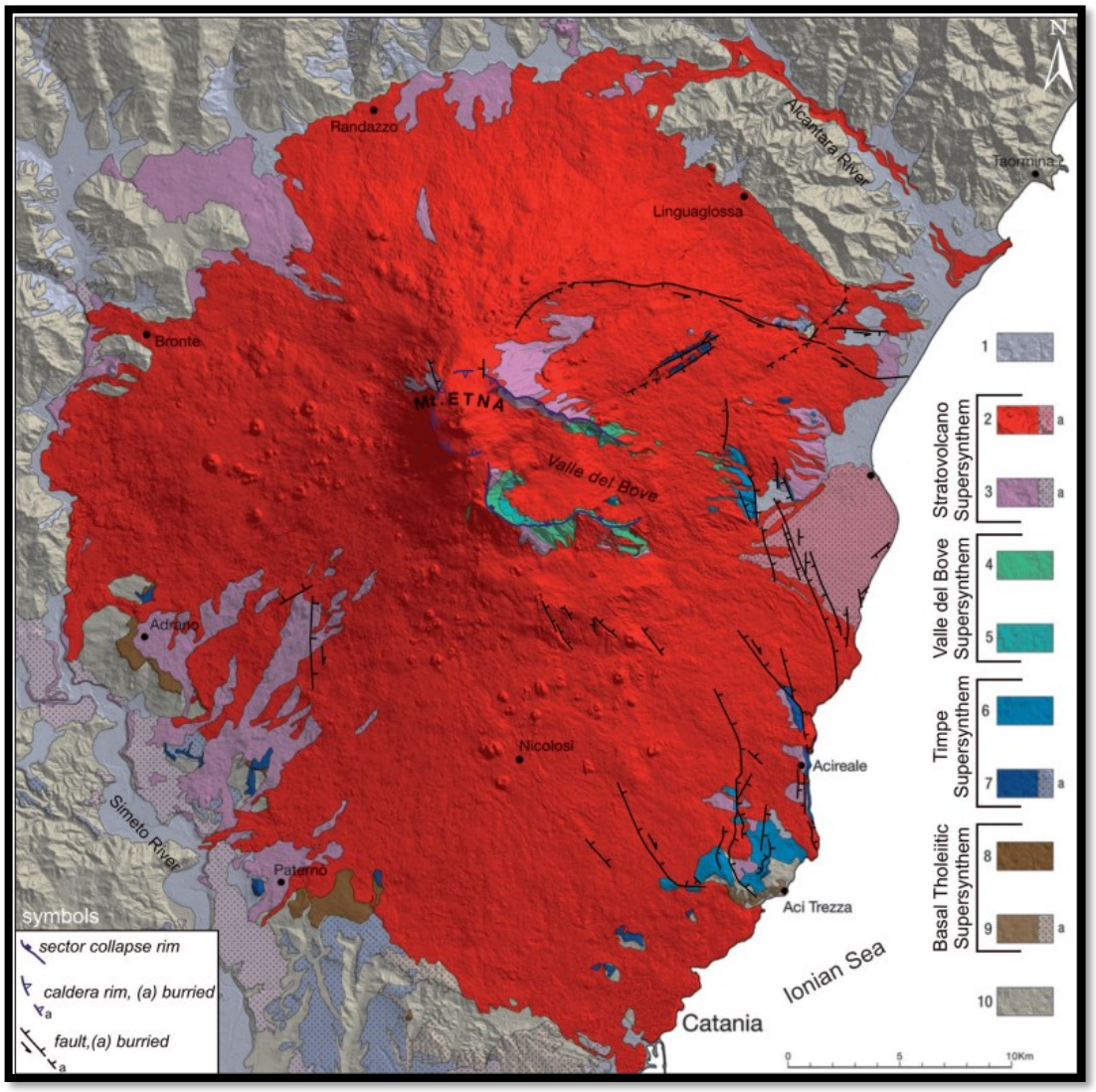

Figure 2: Mt. Etna geological map. major tectono-volcano structure and stratigraphy units by supersynthem classification (Branca, 2011).

Volcanic activity at Mt. Etna is either focused at its four summit craters or occurs from fissures that are mainly concentrated in three so-called rift zones: the NE Rift, the S Rift, and the W Rift (Acocella, 2005). From a structural point of view, the Mt. Etna volcano is characterized by a complex structural setting, related to the regional tectonics on which

the volcano dynamics are superimposed (Branca and Ferrara, 2013). Mount Etna volcano lies at the front of the Sicilian-Maghrebian thrust belt and on the Early-Middle Pleistocene foredeep clayey succession, deposited on the flexured margin of the Hyblean foreland (Barreca et al., 2018). All the lava tube surveys and locations were taken from the book *Dentro il volcano, Le Grotte dell' Etna, 1999*.

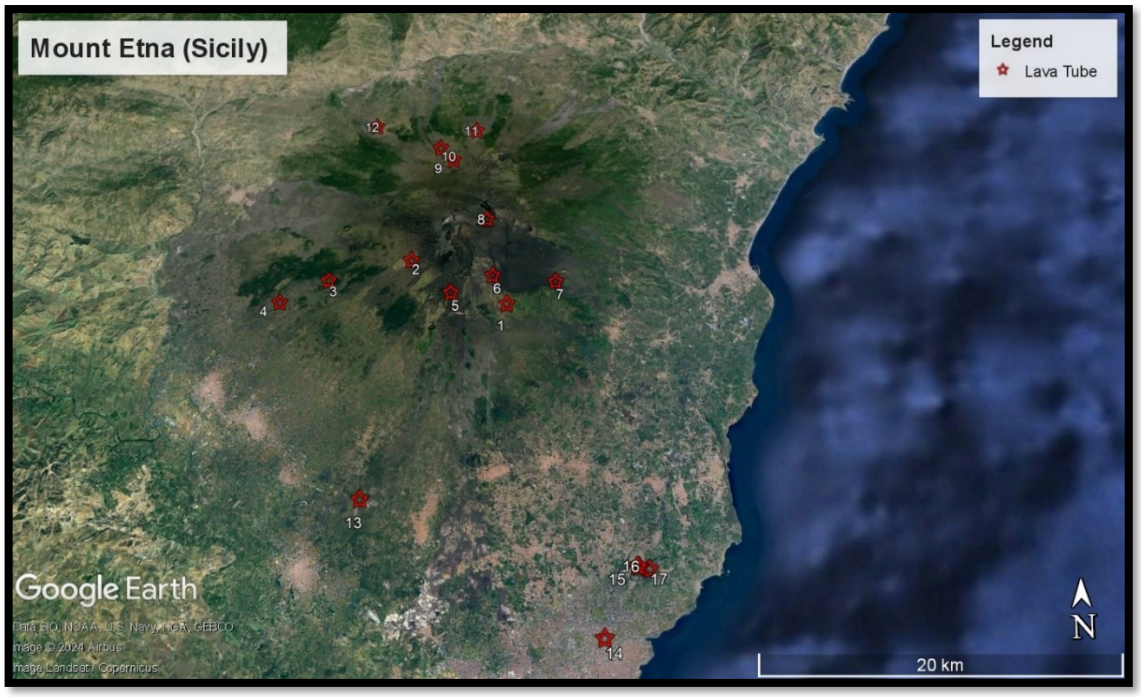

Figure 3: Mount Etna lava tubes ubication. 1)Tre livelli-KTM; 2) Archi Cave; 3) Mt. Intraleo Cave; 4) Santo's Cave; 5) Corsaro Cave; 6) Cutrona Cave; 7) Salto della Giumenta Cave; 8) MA.RA.SCA Cave; 9) Diavolo Cave; 10) Gelo Cave; 11) Lamponi Cave; 12) Burrò Cave; 13) Catanese1 Cave; 14) Nuovalucello1 Cave; 15) Immacolatella1 Cave; 16) Tedeschi Cave; 17) Micio Conti Cave (Bonaccorso and Santi, 1999; Cavallaro F. 1999; Licitra and santi, 1999; Giudice and Santi 1999; Bonaccorso and Cavallaro 1999; Giudice et al., 1999; Marino and Santi 1999; Bonaccorso et al., 1999).

Lava tube	Locality	Morphotype
1)Tre Livelli-KTM	Contrada casa del vescovo, Zafferana Etnea, Mt. Etna (Sicily-Italy)	Single
2)Archi Cave	Bocche eruttive del 1607, Biancavilla, Mt. Etna (Sicily-Italy)	Single
3) Mt. Intraleo Cave	Monte Intraleo, Adrano, Mt. Etna (Sicily-Italy)	Braided
4) Santo's Cave	Contrada Diamante, Adrano, Mt. Etna (Sicily-Italy)	Braided
5) Corsaro Cave	Monte Castellazzo, Belapasso, Mt. Etna (Sicily-Italy)	Single
6) Cutrona Cave	Canalone della Montagnola, Zafferana Etnea, Mt. Etna (Sicily-Italy)	Single
7)Salto Della Giumenta Cave	Salto della Giumenta, Zafferana Etnea, Mt. Etna (Sicily-Italy)	Single
8)MA.RA.SCA Cave	Valle del Leone, Zafferana Etnea, Mt. Etna (Sicily-Italy)	Single
9)Diavolo Cave	Sciara del Follone, Randazzo, Mt. Etna (Sicily-Italy)	Single

10) Gelo Cave	Sciara del Follone, Randazzo Mt. Etna (Sicily-Italy)	Single
11) Lamponi Cave	Feudo Annunziata, Randazzo Mt. Etna (Sicily-Italy)	Single
12) Burrò Cave	Lave del passo dei Dammusi, Castiglione di Sicilia Mt. Etna (Sicily-Italy)	Single
13) Catanese 1 Cave	Passo della Catanese, Ragalna, Mt. Etna (Sicily-Italy)	Braided
14) Nuovalucello 1 Cave	Nuovallucello, Catania, South of Mt. Etna (Sicily-Italy)	Braided
15) Immacolatella 1 Cave	Guardiola Cantarella, S. Gregorio di Catania South of Mt. Etna (Sicily-Italy)	Braided
16) Tedeschi Cave	Guardiola Cantarella, S. Gregorio di Catania South of Mt. Etna (Sicily-Italy)	Braided
17) Micio Conti Cave	Guardiola Cantarella, S. Gregorio di Catania South of Mt. Etna (Sicily-Italy)	Braided

Table 1: Lava tubes from Mount Etna, Sicily, Italy (AA.VV. In: DENTRO IL VULCANO: IL LIBRO Le Grotte dell'Etna, Centro Speleologico Etneo - Parco dell'Etna- Catania, 1999 - pp. 320 + XXI).

2.2-Lanzarote (Canary Islands)

The Canarian Archipelago is a group of volcanic islands within the Atlantic Ocean. They insist on the slow-moving African plate, close to a continental margin (Carracedo, 1998). The Canary Islands Seamount Province (CISP) comprises more than 100 seamounts, isolated volcanic structures on the seafloor ranging from small (<1000 m height) to mid-sized (>1000 m) and mid-sized explosive (<700 m water depth) to ocean islands (Van De Boogard 2013). The intraplate geodynamic settings, developed over a Jurassic lithosphere (150-180 Ma) whose age has been estimated on magnetic anomalies of the ocean floor (Romero & Galindo, 2019). The Canarian archipelago is constituted by seven main island (from East to West: Lanzarote, Fuerteventura Gran Canaria, Tenerife, el Hierro, la Gomera and la Palma), all of volcanic origin (Romero & Galindo, 2019). One of the most studied islands of the archipelago, from the lava tubes point of view, is Lanzarote. This island, with a surface of 846 km2, is the north-eastern extension of the Fuerteventura-Lanzarote volcanic platform, as the sea depth in the narrow *La Bocaina* strait between the two islands does not exceed 40 m. Indeed, Lanzarote and Fuerteventura are the subaerial parts of a single volcano built along a possible fissure striking northeast-southwest parallel to the African coast (Tomasi et al., 2022). Lanzarote may be the longest-lived among the Canary Islands, since the oldest subaerial volcanism is dated at ∼15.5 Ma (Carracedo et al., 1998; Coello et al., 1992; van de Bogaard, 2013; Tomasi, 2022), while the last activity took place in 1824 (Carracedo et al., 1998; Coello et al., 1992; van de Bogaard, 2013). The oldest accessible massifs (Los Ajaches and Famara) are of Miocene age and represent late cycles of a shield stage (Hoernle and Carrecedo, 2009).

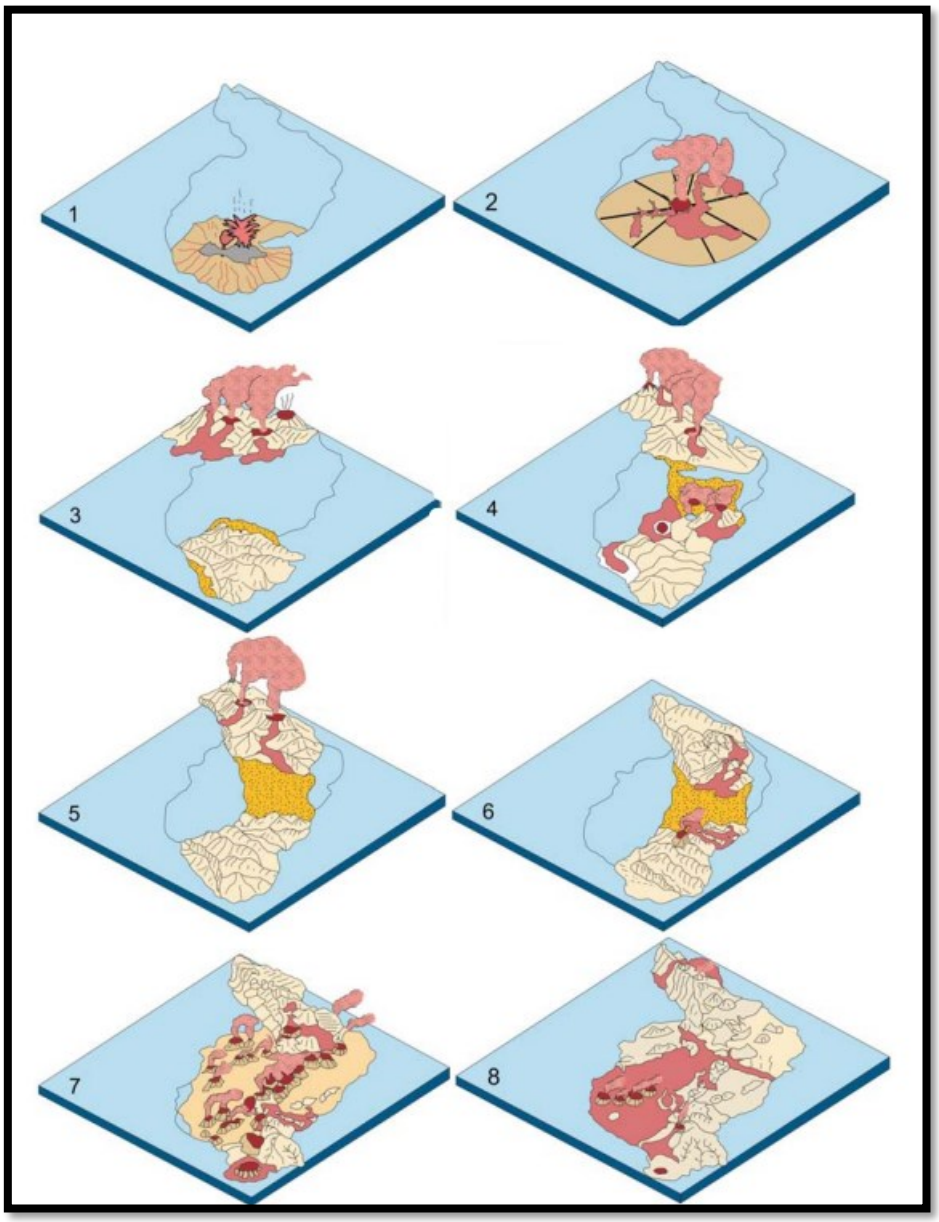

Figure 4: Schematic reconstruction of the evolution stage of Lanzarote, (Hansen and Perez Torrado, 2005).

The physiography of the island is simple; it has two mountain massifs, one in the South (Ajaches) and the other in the North (Famara), with the territories created by volcanic activity over the last 0.8 million years between and partially surrounding them. These volcanic lands are low-lying with very little topographical contrast, with rows of volcanic cones from different times of the mid and early Pleistocene that follow the structural patterns of the NE quadrant (Hansen and Perez Torrado, 2005). The volcanic events that

have occurred over the last 21,000 years, first in the north with the eruption of the La Corona volcano and later in the center of the island, with the eruption of Timanfaya, caused a rejuvenating make-over on an island that was aged and worn down by erosion (Hansen and Perez Torredo, 2005).

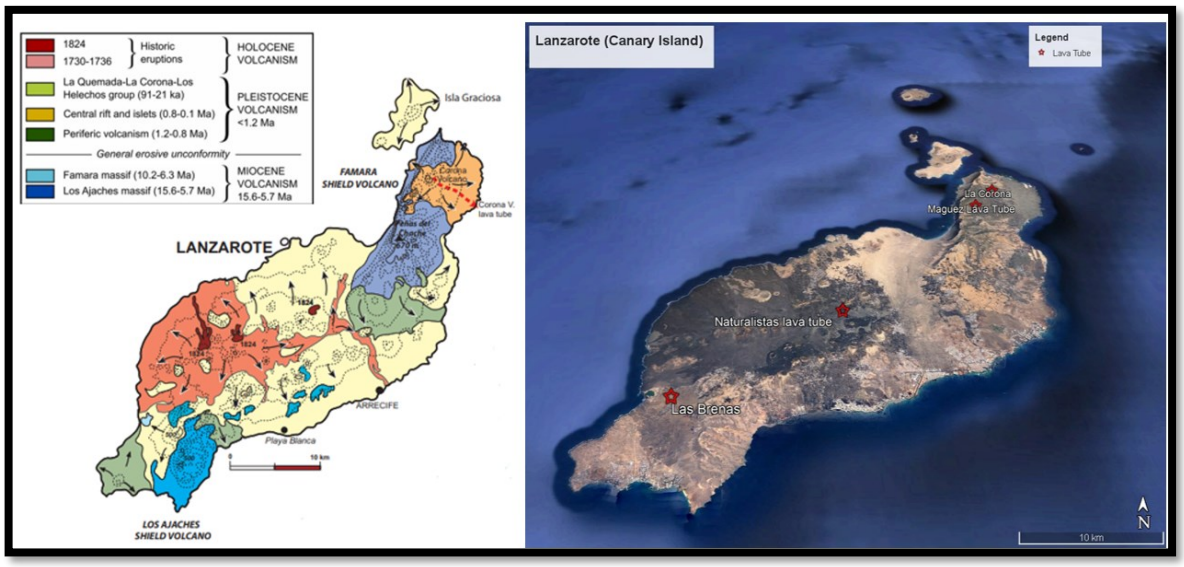

Figure 5: On the left simplified geological map of Lanzarote, Canary Island (modified from Hoernle and Carracedo 2009; Tomasi et al., 2022). On the right are the lava tube locations (modified from Google Earth Pro).

Lava Tube	**Locality**	**Morphotype**
1) La Corona	Peña Redonda, La Corona Volcano, North of Lanzarote (Canary Island)	Single
2) Maguez	Town of Maguez, La Quemada Volcano, Lanzarote (Canary Island)	Braided
3) Naturalistas	Parque Natural de los Volcanes, central part of Lanzarote (Canary Island)	Braided
4)Las Breñas	Town of Las Breñas, South of Lanzarote (Canary Island).	Braided

Table 2: Location and morphotype of the lava tubes from Lanzarote, Canary Island.

2.3-Hawaii (USA)

The seamounts, banks, and islands of the Hawaiian Ridge; and the chain of Emperor Seamounts form an array of shield volcanoes that stretches nearly 6,000 km across the north Pacific Ocean. This unique geologic feature consists of more than 107 individual volcanoes with a combined volume slightly greater than 1 million km^3 (Bargar and Jackson, 1974; Peterson and Moore, 1987).

Hawaiian archipelagos form a southeast-trending line of islands 2400 km long (Mcdonald, 1983). The Hawaii hot spot lies in the mantle under, or just to the south of, the Big Island of Hawaii. Two active subaerial volcanoes and one active submarine volcano reveal its productivity Centrally located on the Pacific Plate, the hot spot is the source of the Hawaii Island Archipelago and its northern arm, the Emperor Seamount Chain (Fletcher, 2008). Volcanism at a hotspot is typically sustained for tens of millions of years, and as the lithosphere moves over the hotspot a chain of volcanoes (a hotspot trace) results (Wilson, 1963).

Hawaiian volcanoes erupt lava of distinct chemical compositions during four major stages in their evolution and growth (Clague & Dalrymple, 1987). The earliest stage is a submarine alkalic pre-shield stage, which is followed by the tholeiitic shield stage. The shield stage probably accounts for >95 percent of the volume of each volcano. The shield stage is followed by an alkalic post-shield stage during which a thin cap of alkalic basalt and associated differentiated lava covers the tholeiitic shield. After several million years of quiescence and erosion, (for the oldest islands of Hawaiian archipelago), very small amount of SiO2-poor lava erupts from isolated vents, this stage is called post-erosional stage or alkalic rejuvenated-stage (Clague & Dalrymple, 1987). Donald W. Peterson and Richard B. Moore (1987) in chapter 7 of the US. Geological Survey Professional Paper identifies the Hawaiian Islands evolutionary sequence:

1. Initial stage. Basanite, alkalic basalt, and lava transitional to tholeiite build a moderately steep-sided edifice from the deep ocean floor.
2. Shield-building stage. Principal development of shield volcano; eruptions are frequent and voluminous from vents in the summit area and along radial rift zones; cycles of caldera formation and related infilling repeatedly develop and the weight of growing edifice causes regional subsidence. Three substages can

be clearly recognized: (*a*) submarine-pillow lavas building moderately sloping submarine edifice; (*b*) sea-level—vigorous interaction between degassing molten lava and ocean waves, lava-steam explosions, hyaloclastite deposits; (*c*) subaerial-pahoehoe and aa lava flows building gently sloping shield volcano while processes of substages *a* and *b* may continue below and at sea level.

3. Capping stage. Alkalic basalt and related differentiated rocks build steeply sloping cap over tholeiitic shield; eruption frequency diminishes, explosive eruptions increase.
4. Erosional stage. The frequency of eruptions declines to zero; stream and wave erosion cuts valleys and cliffs; coral reefs may form offshore.
5. Renewed volcanism stage. After long quiescence, highly differentiated lava and tephra erupt intermittently; erosion and reef-building continue.
6. Atoll stage. The volcano is eroded to sea level and abetted by regional subsidence; the structure is encircled and capped by coral reefs.
7. Late seamount stage. Regional subsidence eventually causes the edifice to sink below sea level, quietly remaining as a seamount. Hawaii's shield volcanoes have broad bases concerning their height and subaerial slopes in the tholeiitic stage, unmodified by faulting or erosion, generally of 3 ° -10 ° and averaging about 6°. Volcanoes with a steeper-sided alkalic cap have summit slopes that locally approach 20° and average about 12° (Peterson and Moore, 1987).

The Island of Hawaii, also known as the Big Island, houses several of the world's most studied lava tubes. The island is the younger surface expression of the hotspot trace, and consists of five quaternary shield volcanoes: Kohala, Mauna Kea, Hualalai, Mauna Loa, and Kilauea, in order of latest activity (Peterson and Moore, 1987). The volcanoes of this Island represent only the first four stages seen before. Kilauea and Mauna Loa are at 2c, Hualalai and Mauna Kea at 3, and Kohala at 4 (Peterson and Moore, 1987).

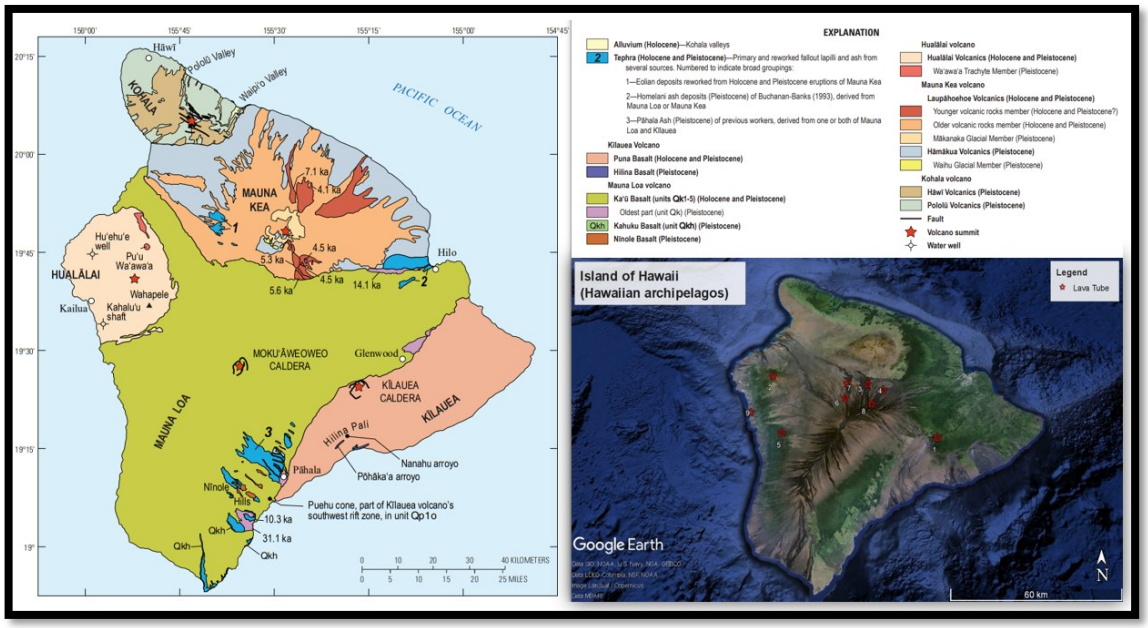

Figure 6: Left map showing stratigraphic formations for volcanoes on the Island of Hawaii (Hawaii- USA), (modified from Sherrod et al., 2021); View of the Island of Hawaii (Hawaii- USA), most of the lava tubes taken in account in this work lies on the N-E flank of Mauna Loa Volcano. 1)Thurston Lava Tube, (Kempe & Henschel, 2008); 2) Manu Nui Cave system, (Bosted and Bosted, 2009); 3) Terraced Cave (Bunnel, 2011); 4) Tusk Cave (Bunnel, 2011); 5) Tom's Hole (Davis, 2009); 6) Sweet Sunday Cave, (Medville, 2008); 7) Lying Eyes Cave (Bunnel, 2011); 8) Hammer Cave, (Bunnel, 2010); 9) Kuamo'o Point Sea Cave (Bosted, 2011). The figure with the lava tube location was modified from Google Earth Pro.

The island of Maui, the second largest of the Hawaiian Islands, consists of two large, coalesced volcanoes, East Maui Volcano (or Haleakala) and West Maui Volcano. Maui's volcanoes are more dissected (being older) than the volcanoes on the island of Hawaii (Langenheim & Clague 1987).

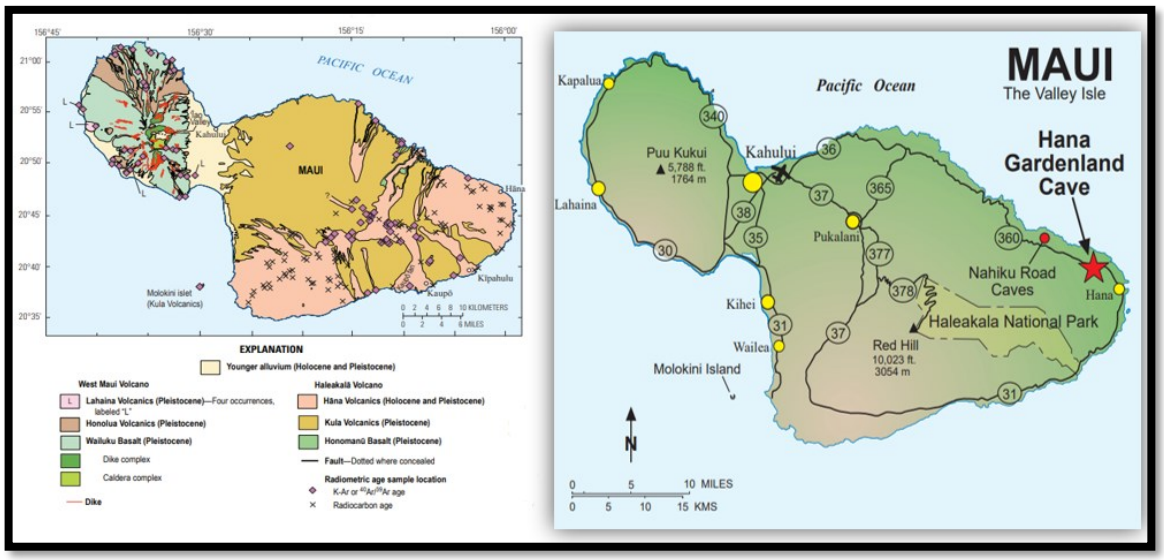

Figure 7: The geological maps of Maui Island (Hawaii- USA) on the left (Sherrod et al. 2021); on the right the location of the Hana Gardenland Cave (Maui Island- Hawaii) on the Est side of the Haleakala volcano, (Richards & Szukalski, 2010).

Lava tube	Locality	Morphotype
1)Thurston Lava Tube	Volcano National Park, Kilauea Volcano Big Island of Hawaii (USA)	Single
2)Manu Nui Cave system	Hualalai Volcano, Big Island of Hawaii (USA)	Braided
3)Terraced Cave	Mauna Loa Forest Reserve-North Hilo district, Hawai'I (USA)	Braided
4)Tusk Cave	North Hilo district, Mauna Loa Volcano Hawai'i (USA)	Braided
5)Tom's Hole	South Kona District, Mauna Loa Volcano, Hawaii (USA)	Single
6)Sweet Sunday Cave	Mauna Loa Forest Reserve (USA)	Single
7)Lying Eyes Cave	Mauna Loa Forest Reserve-North Hilo district, Hawai'I (USA)	Single
8) Hammer Cave	South Hilo district, Mauna Loa Volcano, Hawaii (USA)	Single
9) Kuamo'o Point Sea Cave	South Kona District, Mauna Loa Volcano, Hawaii (USA)	Single
10) Hana Gardenland Cave	Haleakala Volcano, Maui Island, Hawaii, (USA)	Braided

Table 3: Location and morphotype of the lava tubes from Hawaiian archipelagos, USA (HSS Newsletter, National Speleological Society).

2.4-Galapagos

The Galapagos Archipelagos lies in the central East Pacific Ocean, just south of the Cocos-Nazca spreading center (CNS) also known as the Galapagos spreading center (GCS) (Werner et al. 2003). The archipelago is the surface expression of a hotspot or long-lived mantle plume whose interplay with the Galapagos spreading center during the Neogene has resulted in the formation of two hot spot tracks, the Cocos and Carnegie Ridges, and associated seamounts on the Cocos and Nazca Plates, respectively (Werner et al. 2003). The GSC has migrated northward away from the hotspot in the last 5-6 Ma, judging from the volcanic traces of the hotspot, the Cocos and Carnegie ridges (White et al. 1993).The presently active Galápagos hotspot has produced several voluminous shield volcanoes, most of which have been deactivated by the ESE movement of the overlying Nazca oceanic plate (Kempe, 2021). The Galápagos plume was formerly juxtaposed with the Galápagos spreading center (GSC), and concurrently contributed to the production of the Cocos and Carnegie ridges, on the separating Cocos and Nazca plate, but they have drifted apart over the past ~8 Ma with the plume center, now south of the GSC, beneath the island of Fernandina (White et al. 1993; Wilson and Hey 1995; Kelly and Salazar, 2017).

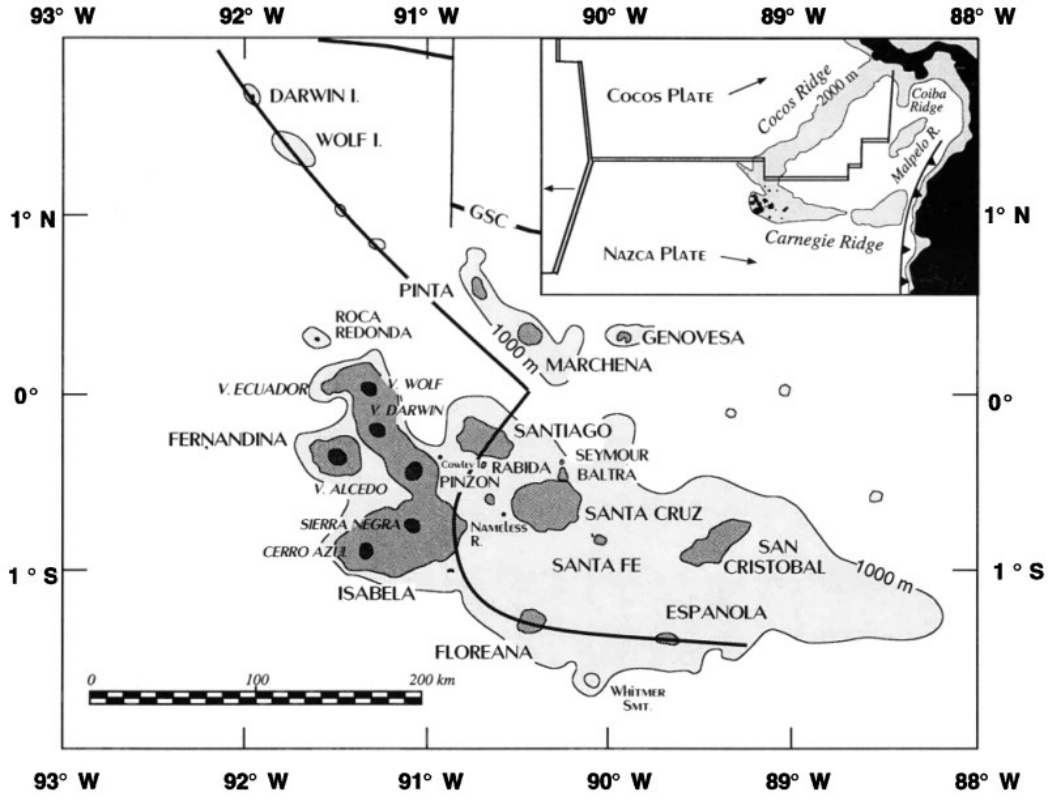

Figure 8: Map of the Galapagos Archipelago. GSC is the Galapagos Spreading Center. The bold line shows the lithospheric fault system that separates thin, weak lithosphere to the north and east from stronger and thicker lithosphere to the south and west inferred by M. A. Feighner and M. A. Richards (submitted manuscript, 1993). Inset shows the regional tectonic setting (White et al. 1993).

The main Galápagos Islands are located east of the N-S trending East Pacific Rise and south of the E-W-trending Galápagos Spreading Center and some 1,000 km west of the Ecuadorian mainland (Kempe 2021; Werner et al. 2003). Of the 21 emergent volcanos in the Galapagos, nine have been active historically and four others have erupted in the Holocene and should be considered still active (White et al. 1993). Generally, the ages of the islands younger westward to older (~5.5 Ma) in the eastward. Most of the historic eruptive activity is indeed in the western islands, but some young lavas are present throughout the archipelago (White et al. 1993). Santa Cruz is a gently sloping, elliptical shield rising 950 m above sea level. A series of youthful pyroclastic cones and pit craters is aligned along a WNW trending axial fissure system defining the summit of the volcano (White et al. 1993).

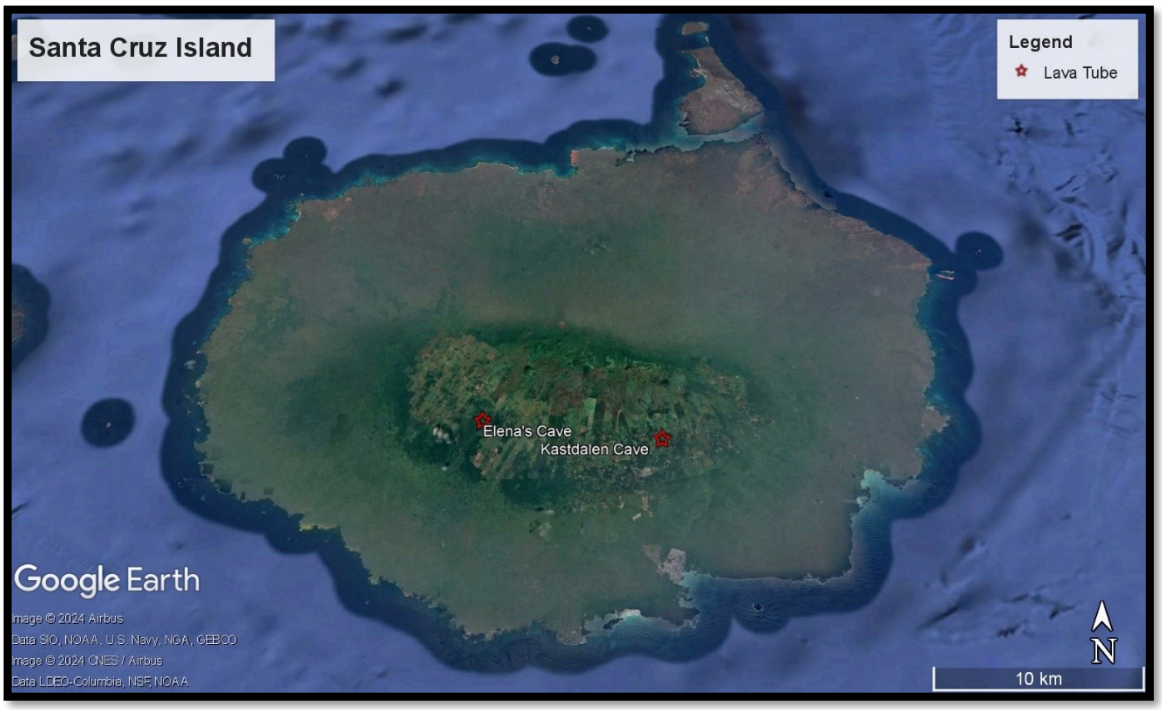

Figure 9: Santa Cruz Island, Galapagos. From east to west, la Cueva de Elena and la Cueva de Kastdalen, are the only two caves taken into account for the Galapagos Archipelagos (modified from Google Earth Pro).

Lava tube	**Locality**	**Morphotype**
1)Kastdalen Cave	Santa Cruz Island Galapagos (Ecuador)	Single
2) Elena's Cave	Santa Cruz Island Galapagos (Ecuador)	Braided

Table 4: Location and morphotype of the lava tubes from Santa Cruz Island, Galapagos, Ecuador (Gallardo, 2008).

2.5-Iceland

Geographically, Iceland is located at the intersection of two oceanic ridges, the MidAtlantic Ridge separating the North American and the Eurasian lithospheric plates on one hand, and the series of ridges connecting Greenland and Iceland, Iceland and the Faroe Islands, and continuing to the United Kingdom (Eiríksson, J., & Símonarson, L. A. 2021). This island is an exceptional natural laboratory to study interactions between magmatism and extensional tectonics (Dauteuil, O., & Bergerat, F., 2005), it lies in the North Atlantic igneous province (NAIP). Volcanism within the North Atlantic igneous province (NAIP) was initiated at c. 61 Ma, with massive volcanic activity extending from northern Canada to Scotland between 61 and 56 Ma (Storey et al., 2007; Eiríksson, J., & Símonarson, L. A. 2021). During the initial phase of volcanism in the NAIP (61 Ma), dominantly Basaltic magmas were erupted from beneath thick continental lithosphere simultaneously in a circular area about 2000km in diameter (Storey et al., 2007). Volcanic activity was increasingly intermittent by 57-56 Ma, but at 56.1±0.5 Ma the average melt production rate increased by more than an order of magnitude over previous levels, coinciding with continental rifting and shallow decompressional melting of the mantle (Storey et al., 2007). Nowadays the volcanism of NAIP is focused and higher in Iceland than along the spreading axes to the south and north, indicating a mantle anomaly beneath the island, a hot spot (Eiríksson, J., & Símonarson, L. A. 2021). The Topography of Iceland forms a large bulge on the North Atlantic Ocean floor, features that generally reflect an anomaly in the mantle below, a stationary hotspot beneath Iceland (Eiríksson, J., & Símonarson, L. A. 2021). Indeed, Greenland-Iceland-Faerores ridges represent a hot-spot trail that may have been partially above sea levels, a theory supported by some work of paleobotanic by Grimsson (2007). The existence of the Icelandic Plume is still debated, Celli's (2021) work, using tomography, reconciles previously contrasting views on the structure of the Iceland Plume: while the plume is clearly visible in the transition zone beneath Greenland, it is confined to the upper mantle beneath Iceland. Icelandic bedrock is subdivided into four main chronological successions (Thordarson, T., & Larsen, G. 2007).

1. The Holocene e late glacial succession 0 – 0.015 Ma.
2. The upper Pleistocene succession 0.015 – 0.78 Ma.
3. The Plio-Pleistocene succession 0.78 – 3.3 Ma.
4. The Tertiary succession 3.3 – 16 Ma.

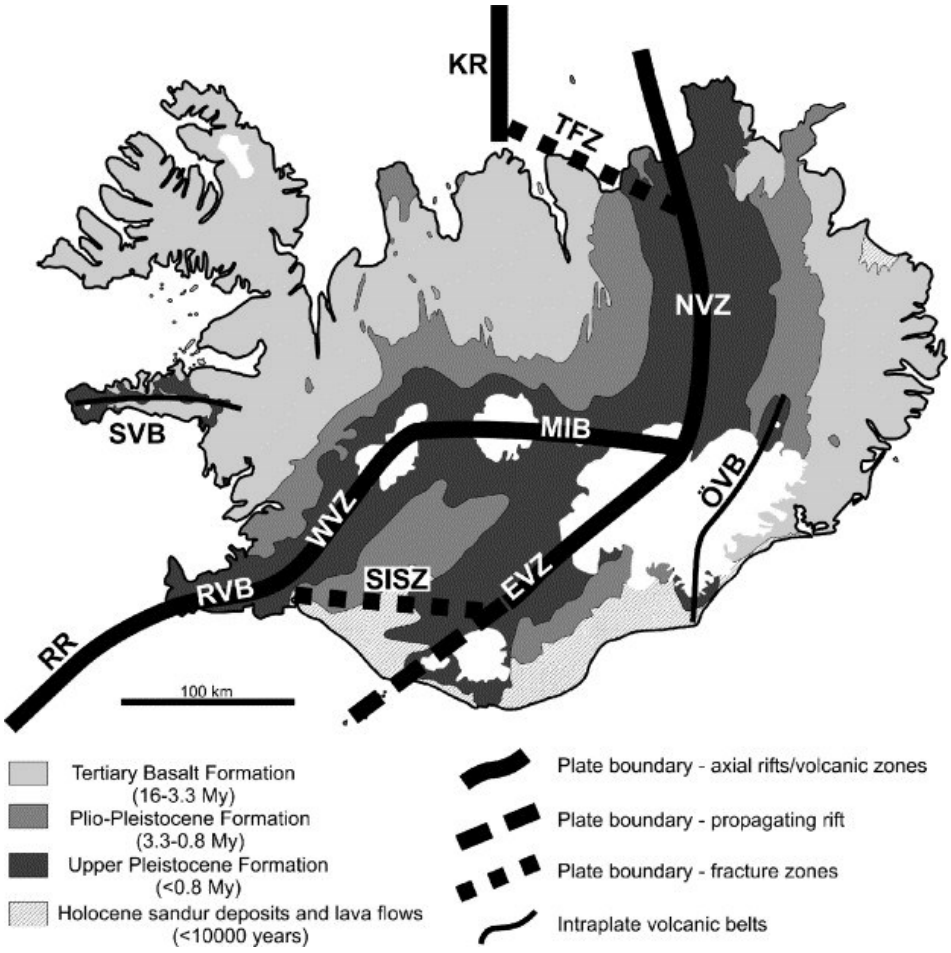

Figure 10: The principal elements of the geology in Iceland, outlining the distribution of the major geological subdivisions, including the main fault structures and volcanic zones and belts. RR, Reykjanes Ridge; RVB, Reykjanes Volcanic Belt; SISZ, South Iceland Seismic Zone; WVZ, West Volcanic Zone; MIB, Mid-Iceland Belt; EVZ, East Volcanic Zone; NVZ, North Volcanic Zone; TFZ, Tjörnes Fracture Zone; KR, Kolbeinsey Ridge; ÖVB, Öræfi Volcanic Belt; SVB, Snæfellsnes Volcanic Belt (Thordarson, T., & Larsen, G. 2007).

Systematic mapping has been carried out in many Tertiary areas on a regional scale, the bulk of these are made up of subaerial tholeiitic flood basalt separated by minor clastic interbed, usually of volcanic origin (Thordarson, T., & Larsen, G. 2007). Is possible to distinguish two kinds of volcanoes, crater rows, and lava shields (Thordarson, T., & Larsen, G. 2007).

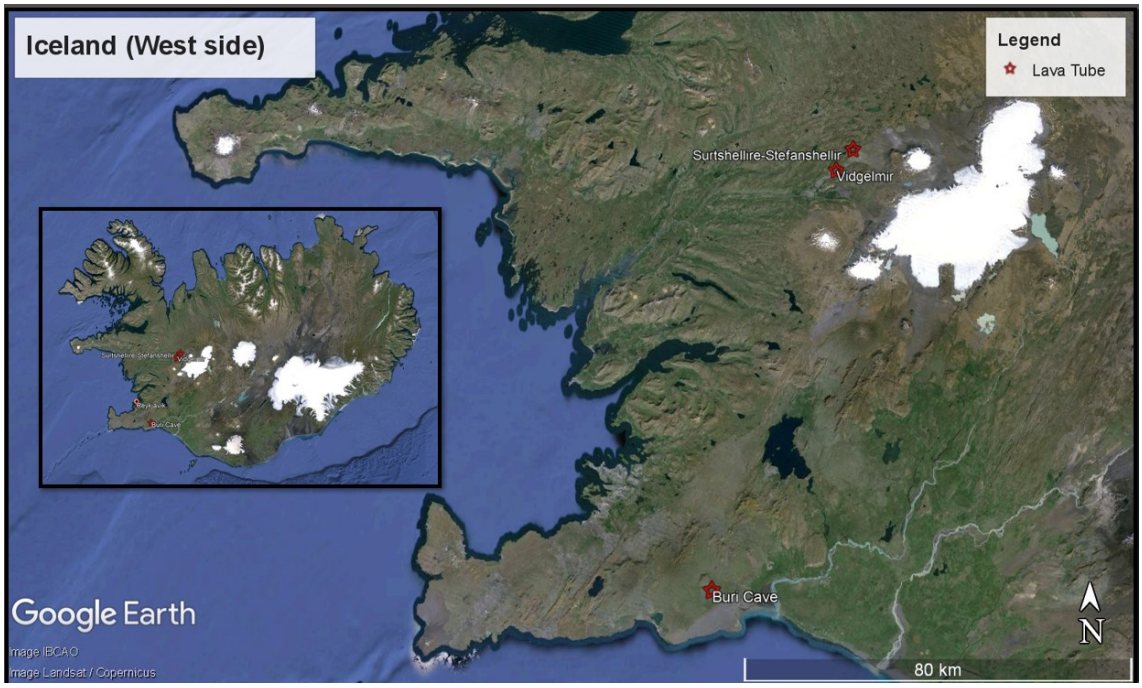

Figure 11: Iceland's west side, the three lava tubes taken for this work: Buri, Viðgelmir, and Surtshellir-Stefanshellir (modified from Google Earth Pro).

Lava tube	Locality	Morphotype
1) Viðgelmir	Hallmundarhraun lava flow field, Iceland	Single
2) Buri	Leitahraun lava flow field, south of Reykjavik, Iceland	Single
3) Surtshellir-Stefanshellir	Western flank of the Langjökull glacier, Iceland	Braided

Table 5: Location and morphotype of the lava tubes from Iceland (Hróarsson B, 2006).

3-Lava Tube Morphologies

As we seen in the introduction chapter, lava tubes can show many different patterns and morphologies, often related to genetic processes, effusion rate or paleo-topography. Usually, *overcrusted* tubes are limited to the width and depth of the channels where they originally formed, with roofed sections not exceeding few tens or maximum hundreds of meters in length and a few meters in diameter (Sauro et al., 2020). Lava tubes formed by shallow inflation are usually characterized by a superficial bulge (due to the inflation) along its development, and by an original horizontal elliptical cross-section that can be eventually entrenched by thermal erosion (Sauro et al., 2020). In addition to *overcrusted* and shallow inflated lava tubes, few cases on Earth have been proposed as a very peculiar example of "deep inflated-entrenched" lava tubes (Sauro et al., 2020). These formed through inflation along deep inception horizons following previous lava flow boundaries where, after inflation, the conduit has been enlarged by downward thermic erosion and breakdown phenomena. Deep-inflated lava tubes are characterized by no surface expression (Sauro et al., 2020). The main patterns for lava tubes are, single tube, sinuous or rectilinear, braided with splitting and reconnection (Sauro et al., 2020), loop morphology, or branches that developed in different directions. The multi-level feature are related to different levels connected by lava falls, shafts (Sauro et al., 2020), or often by internal skylights.

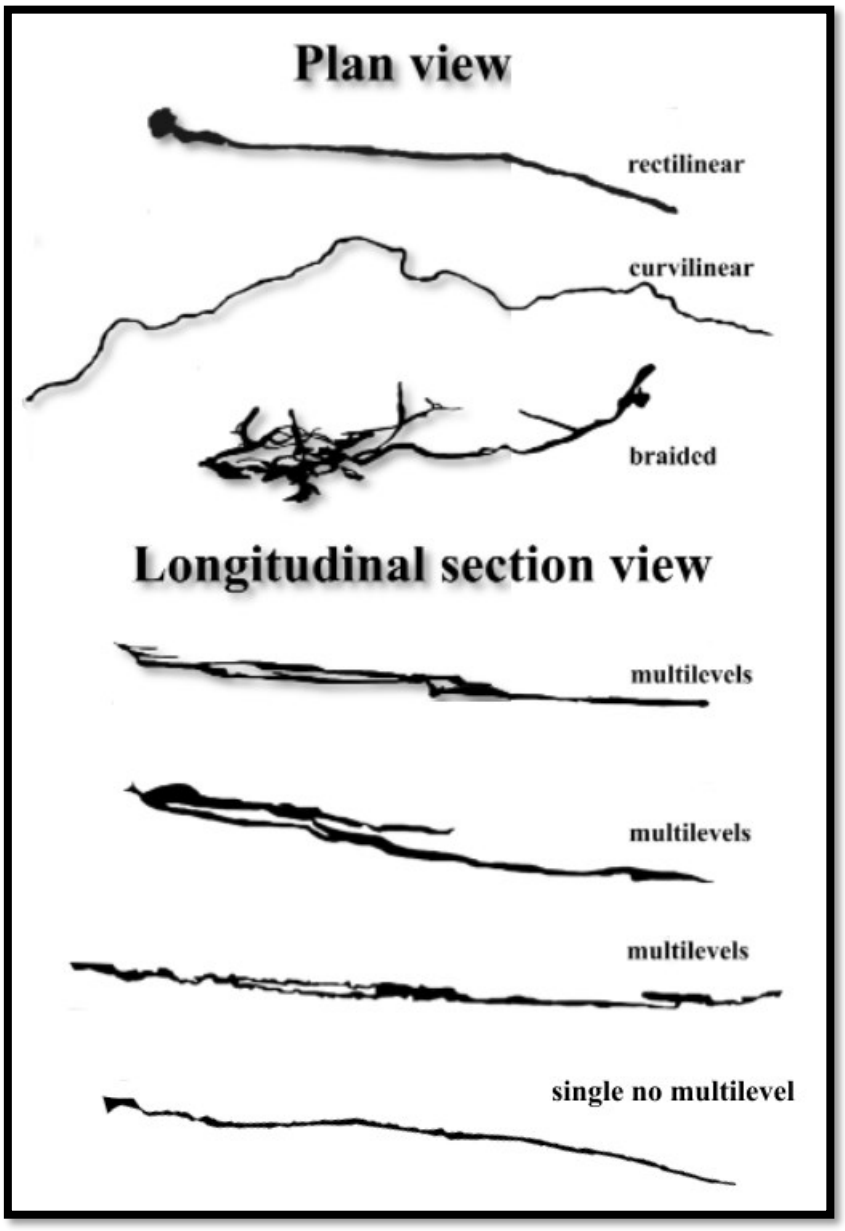

Figure 12: Patterns of lava tubes on caves surveys. Single rectilinear, single curvilinear or braided, visible on plan view. Multi-level structures are detectable on the longitudinal section. The sketches are not in scale (modified from Inkscape).

The most important features of many longitudinal profiles of lava tubes are the alternation of very wide chambers and narrow, low passages (Calvari and Pinkerton, 1999), in addition, many other features can be extrapolated from the longitudinal section. The cupola, lava falls, and multi-levels are detectable on the longitudinal section, while the cave map shows the pattern of the tube, their sinuosity or rectilinear path. In addition, the size of the lava tubes as for lava flow is controlled by the effusion rate, and from the

maintenance of this rate for a certain length of time. (Wadge, 1978). Hence, with increasing of the effusion rate a long and width tube develops. From Kempe (2012), three main morphotypes of lava tubes were described, (1) Single-trunked systems; (2) double (or multiple)-trunked systems; and (3) superimposed-trunked systems. Single-trunked systems are fed by one eruption vent and their size depends on the lava discharge rate (effusion rate) and on the length of activity (eruption time). Double-trunked systems are comprised of two lava tunnels fed by two separated eruption points, the interaction of such tunnels leads to more complex morphologies.

Superimposed-trunked system is defined as a set of tunnels superimposing and crossing each other, all being active at the same time. While these patterns could be detected by observing lava tube surveys, other morphologies, like lateral benches, and lining walls, being details often not shown in surveys, can be recognized only by field observation.

Lining walls these are thin layers of lava covering the conduit walls (Bunnel, 2013; Tomasi, 2022). Sometimes, due to their collapse pre-existing lava flow sequences including potential, pyroclastic layers are brought to light. According to Tomasi et al., (2022), these weak pyroclastic layers are preferential horizons for tube emplacement, and in some cases, facilitate the deep-inflation processes.

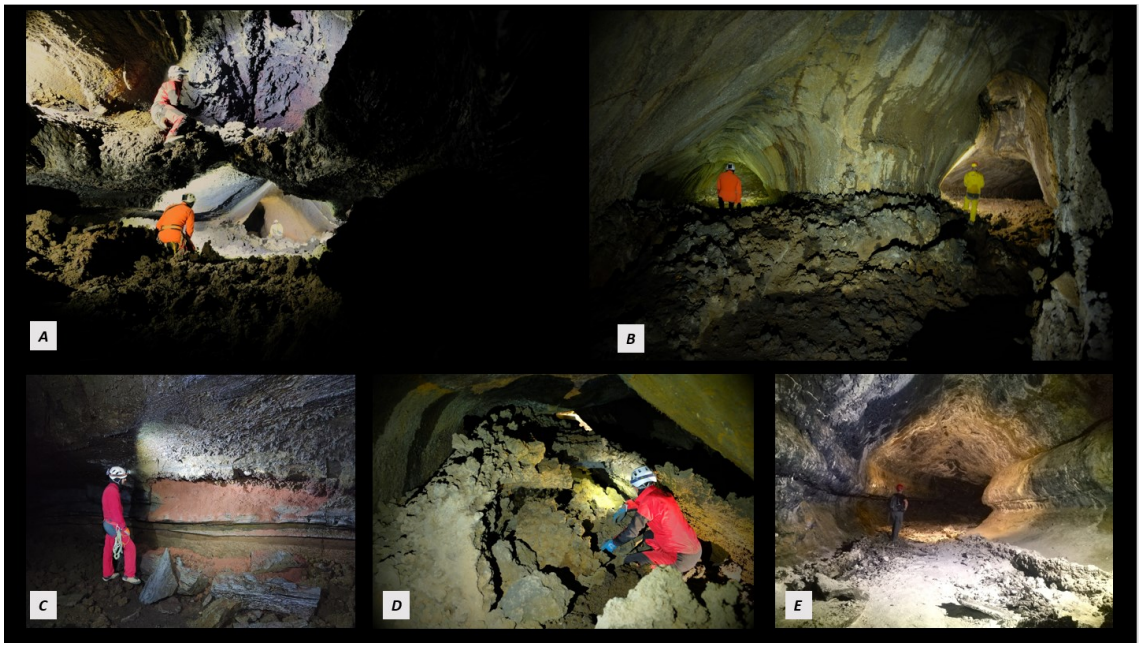

Figure 13: Morphologies and particularly features of lava tubes. A) formation of multi-levels in Tre livelli-KTM (Mt. Etna) due to levees closure (inside overcrusting); B) Tubes split into different branches inside Monte Intraleo cave (Mt. Etna); C) lining wall collapse inside Tre livelli-KTM cave showing an underlying red pyroclast layer; D) Tube-in-Tube in the upper part of the Monte Intraleo cave (Mt. Etna); E) Flow ledges inside the la Corona lava tubes (Lanzarote-Canary Island) and a tube-in-tube structures on the floor.

The lining walls preserve a record of periods when lava partially or completely filled a lava tube (Calvari and Pinkerton, 1999). The lateral benches, also known as flow ledges, indicate a stable lava level maintained for long enough to allow lateral solidification (Calvari and Pinkerton, 1999) and accretion. In addition, if this level remains stable long enough, the benches will join, forming an upper level, often connected to the lower one by a window (Tomasi et al., 2022). Two main morphologies follow these processes, the multi-level or the tube-in-tube structures (Kempe, 2012; Tomasi et al 2022). The latter occurs when a small tube forms on the floor of a pre-existing lava tube (Tomasi et al., 2022). The Flow ledges have a terraced-shape due to lava accumulations, preferentially formed at the external (colder) walls of meandering lava tubes (Tomasi et al 2022).

Knickpoint in longitudinal section show the lava falls, often related to the thermo-mechanical erosion of the tube footwall. In association with knickpoints or enhanced tube curvatures, cupolas can develop in the tube ceiling (Tomasi et al 2022). Peel-off and

rolling-over structures (Calvari and Pinkerton, 1999), are related to the ductile behavior of the lava walls after the emptying of the tube, some layers of lava that are still ductile break away from the walls and may roll in on themselves. Something similar could happen to the roof, where the hot lava starts to drop downward forming stalactites and stalagmites. As for lava channels, also for lava tubes the shape of the cross-section depends upon flow conditions during its formation and the physical properties of the lava and substrate and could in principle be used to provide additional constraints upon flow conditions (Jarvis, 1995), and genetic processes. An examination of transverse sections of primary lava tubes and their modification with distance from the source is essential in understanding the mechanism of flow development (Calvari and Pinkerton, 1999). Indeed, the shape of the cross-sections could tell something about genetic processes for lava tubes. The aspect ratio is an important value to describe the shape of the cross-sections. The cross-sections shapes of lava tubes are usually arched (with various type of angle), round, oval, or alternatively keyhole shaped, due to the accretion of lava to the sidewalls along flow ledges and/or down-cutting by thermal and physical erosion (Allred and Allred, 1997; Greeley et al., 1998; Fagents and Greeley, 2001; Sauro et al, 2020; Tomasi et al. 2022). Regarding “overcrusted” lava tubes, it is also possible to see an approximately rectangular shape, due to the way of channel closure. The blocks, lavaballs and secondary clasts of already solidified lava, form a “log jam” on the surface of a channelized lava flow, lead to the closure of the channel (Kempe, 2010). Differently, if lava channel get closure by lateral shelf growth, the cross-section shapes it’s one resembling an upside-down light bulb (Calvari e Pinkerton, 1999; Baylei et al. 2006; Kempe, 2010).

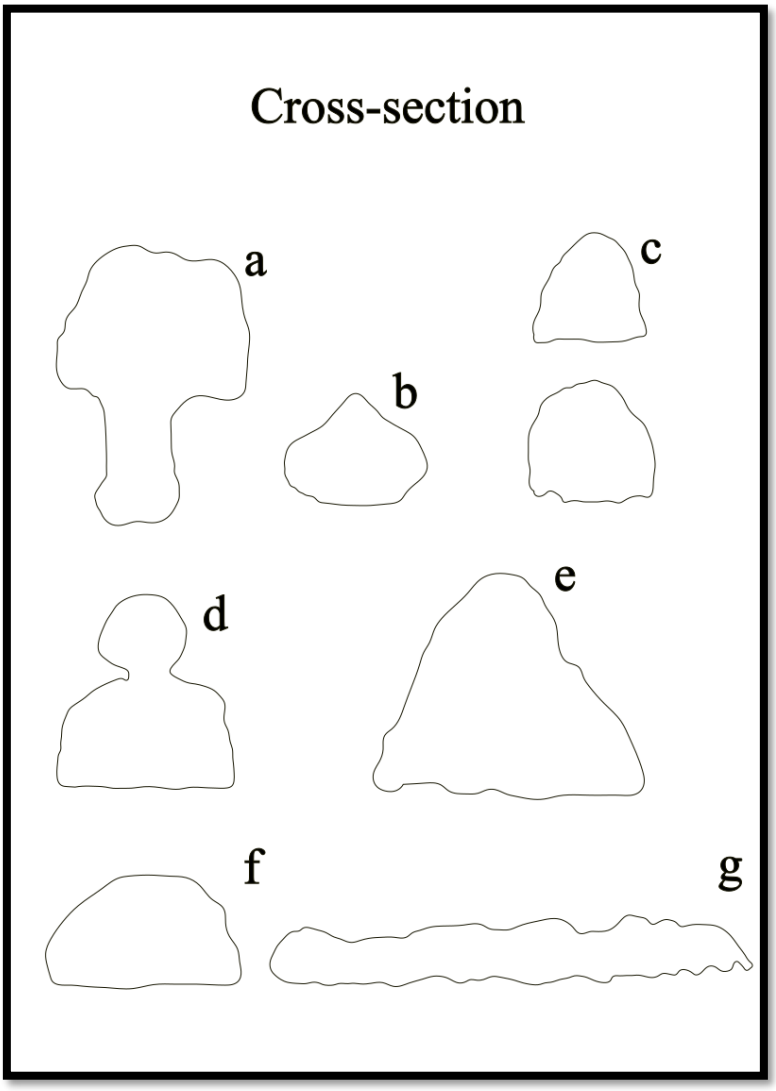

Figure 14: Cross-section shape and geometries. a) keyhole shape due to flow ledges growth or thermos-mechanical erosion of the floor; b) upside-down light bulb shape, typical of flow ledges closure in overcrusted lava tubes; c) multi-level cross-section related to the flow ledges connection due to the decreasing of effusion rate; d) keyhole shape due to flow ledges growth without junction of these, inside a pre-existing lava tube; e) triangular shape related to flow ledges growth; f) rectangular shape, typical of the overcrusted due to agglomeration of floating clasts; g) elongated cross-section related to shallow inflation (modified on Inskape).

The Aspect ratio may be a marker of lava tube evolution and genetic processes, in the case of the lava flows, was not found a relationship among aspect ratio and slope. (G. Wadge, 1978), we can state the same for lava tubes. Hence, we would expect that as for lava flow, it is merely the effusion rate that affects the aspect ratio of lava tubes. Instead, the evolution of lava tubes leads to cross-sectional reshaping, especially when caves suffer a multiphase evolution. A first distinction through the observation of cross-section shapes, was made by Calvari and Pinkerton (1999), on Etna lava tubes, they subdivided into two main groups, simple and compound lava tubes. The shape of the cross-section may denote the possible coalescence between two tubes, the coalescence could be lateral (Calvari and Pinkerton, 1999), while deep canyons can form due to thermal and mechanical erosion (Sauro et al., 2020; Tomasi et al. 2022). Sometimes, due to specific topographic settings (abrupt change in slope) or effusion rates (decreasing of effusion rate), flow ledges can be connected, forming two or more levels of tubes, as we see in lava channels with levees connection. Many of these morphologies seem to refer to a particular topographic setting and or to specific genetic processes, so finding these features could help to identify the genetic processes of lava tubes and their complex evolution.

4-Methods:

In this chapter, I will present the methods adopted in this work to extract the parameters and indices and their significance.

4.1-Digital processing

In this work, I have considered 36 lava tube surveys from five different regions of the Earth: Etna, Lanzarote, Hawaii, Galapagos, and Iceland. In particular, it was decided to use only complete surveys of cavities with plan length greater than 100 meters. Several speleological teams use “disto X”, a laser meter allowing fast and precise measurements, alternatively, surveys were made using clinometers, compasses, and tape meters. Survey precision is controlled by human factors. Indeed, the data quality could be affected by possible errors due to digitalization processes, or due to the way of reporting the survey data to the final sketch. The first kind of error, often related to the adopted scale, can be identified and solved, the second one is harder to detect and in this case, the survey need to be carried out a second time. A remarkable example of this case is the Cueva di Elena (Santa Cruz Island, Galapagos), for which two surveys are available, one from Gallardo (2008) and the other from Hernandez et al., (1991). Gallardo's survey, showed a huge difference in plan length (see following chapter 4.2) measured on the survey, compared to the data expressed in the cave inventory, whereas Hernandez’s survey after digitization returns measurements in line with the data on the cave inventory. Once the surveys were retrieved, I began their digitalization. Extrapolating morphometric indices is a complex and time-consuming task, plus, the resolution of the file does not always allow simple digitalization. Most of the surveys were in image files, such as *.PDF* or *.PNG*, so it was necessary to transform them in vector files (DWG or DXF). Graphics software, such as AutoCAD (2012 version), allowed to visualize image files and transform them into vector files. Before the transformation into vector files, I fixed the scale using the scale bar present as a reference, in each survey. Once the scale was fixed, I used the polyline tool to draw the maps in planar view and the related sections by reconstructing the walls, roofs, and floors of the caves.

4.2-Morphometric parameters and indices

Dimensional parameters such as plan length negative or positive drop, are often found within the survey, other parameters were instead extrapolated. To measure all the dimensional parameters, I used AutoCAD and Q-gis software (https://download.qgis.org) while the indices were derived using Excel sheets. Lava tube maps and sections were measured to determine the following parameters (Table 6): plan length (**Pl**), vertical range (**Vr**), real length (**Lr**), area of the plan map (**Ap**), area of the section **(As**), average interior width (**Wa**), average interior height (**Ha**), short axis (**S**), long axis or extension (**Es**), Length of the longitudinal section (**Ls**). From these dimensional parameters, we can obtain several morphometric indices, but what do these parameters mean, how do they describe the cave? The most common dimensional parameter is the plan length (Pl), that is the length of the cavity measured on the planar map of the cave, not considering the vertical sections and the inclination of the conduits. The negative and positive drops are measured on the longitudinal section from cave entrance to the highest and lowest explored points respectively. The sum of negative and positive drops is the real vertical range (**Vr**) of the cave. Differently from plan length the cave real length (**Lr**) is the sum of all the polygonal chain segments, which consider also slope and shaft (i.e., inclined, and vertical segments). The area of the plan map (**Ap)** and area of longitudinal section (**As)** are measured in the same way, the first one on the planar view map, while the other on the longitudinal section. The average interior width (**Wa**) is calculated dividing the area of the planar view map by the plan length of the tubes (**Ap/Pl**). The average interior height (**Ha)**, was calculated rationing **As** on **Lr**, in some cases, the longitudinal section is only refer to the main gallery, for this reason, I took into account the length of the longitudinal section (**Ls**) present in the surveys, which is not always the real length of the cave. The last two parameters are the long axis or cave extension (**Es**) and the short axis (**S**), both measured as the long and short side of the minimum oriented rectangle including the planar view of the cave (see Figure 16).

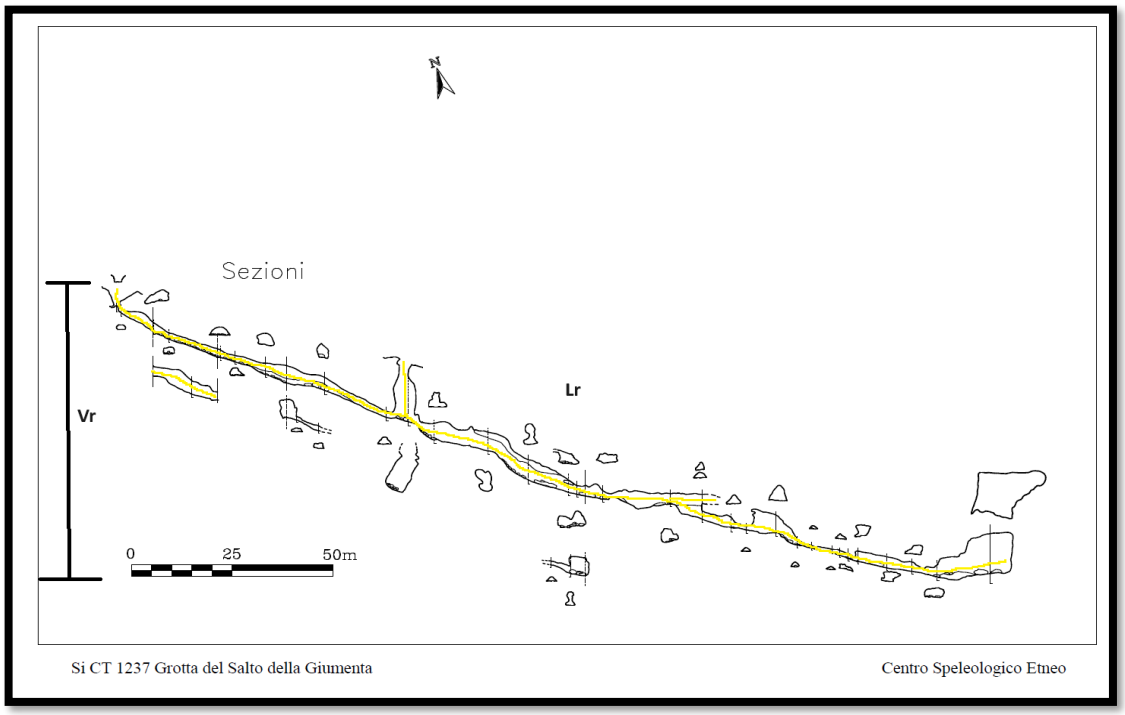

Figure 15: example of the extraction of dimensional parameters from the longitudinal section of the tube "Grotta del Salto della Giumenta" Mt. Etna, (Bonaccorso et al. 1999), vertical range, (sum of positive and negative drop) (black line), and real length (yellow line).

Klimchouk (2023) suggest to compare the volume of the caves, obtained by multiplying the plan map area (**As**) by the mean height of the cave (**Ha**). Sauro et al. (2020) propose the tube linear volumes (**aLV**). This value is derived assuming an elliptical cross-section of the conduits and following the equation [(**Ha**/**2**)*(**Wa**/2)] * π, whose value is multiplied by the real length (**Lr**). We measured the "*Cave field"*, using the minimum rectangle including the entire cave system in the planar map (Fig 16). This parameter was obtained using Qgis software through the Bounding Box tool. The above mentioned parameters allow us to derive four important indices such as:

1. *Areal coverage* - is the area of the cave itself over the area of the Cave field.
2. *Specific Volume*- the volume/length ratio, which characterizes the average size of the cave passage.
3. *Passage network density* – is the ratio of the length over the area of the cave field.

4. *Cave Porosity:* is the volume of the cave divided by the volume of the "Bounding Box", which is the area of the cave field by the vertical range. The cave porosity is expressed as a percentage.
5. *Average Aspect Ratio (Ar)* – is the ratio of average width (**Wa**) over average Height (**Ha**) of the caves average cross-section.
6. Some other morphometric indices, taken from Piccini (2011) are:
7. Ap/Pp: Area of the plan map over the Perimeter of the plan map.
8. S/Es – Short axis over Extension (long axis).
9. Box fill – cave area over the area of the cave field in percentage.

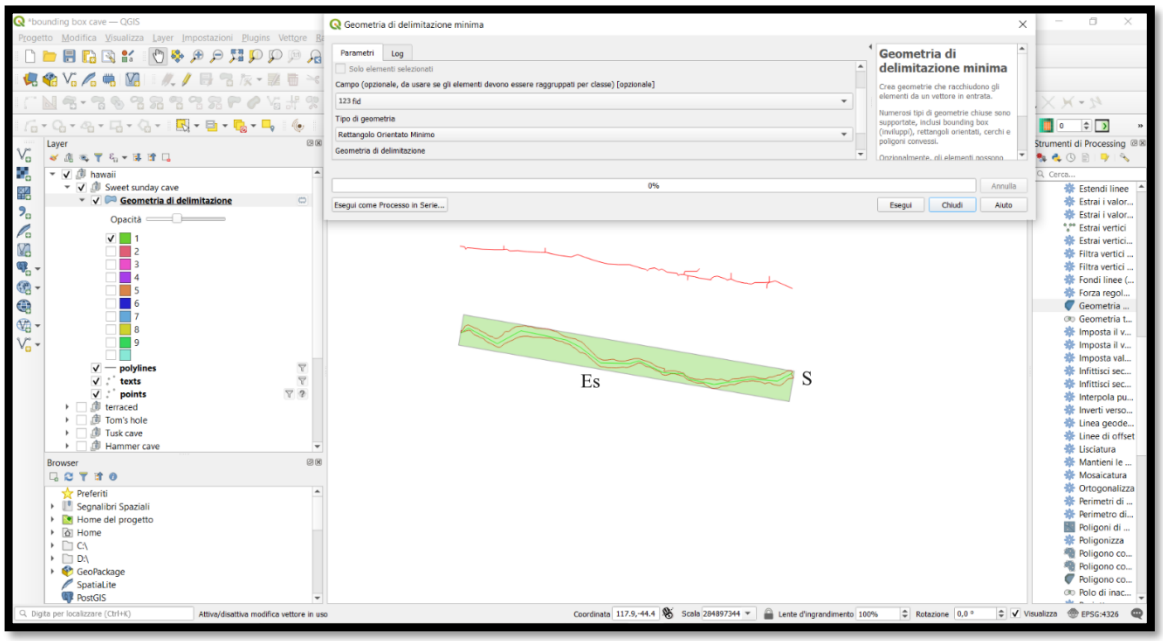

Figure 16: extraction of the cave field by using geometry of minimum bounding tool, trough the minimum oriented rectangle rule. The long side is the Extension of the cave while the short side is the short axis. Sweet Sunday cave (Island of Hawaii- Hawaiian Archipelagos) maps, obtained from AutoCAD and imported on Q-gis software.

Combining of the dimensional parameters seen in the previous chapter, allows us to obtain some morphometric indices. Many of the indices was taken from Piccini (2011), designed for karst caves, but equally useful in describing lava tubes. The indices could be compared with other dimensional parameters or indices, in order to obtain significant correlation.

Vertical index *(Vi)* = Vr/Lr

The vertical index has a theoretical range from 1 to zero, a perfect vertical pit has Vi~ 1.

It's a measure of how close the pits are one each other, and can be a measure of the effect of the structural features on the cave patterns. For lava caves this index is useful to discern lava tubes from fissural cavities and secondary vents (Piccini, 2011).

Horizontal complexity index *(Hci)* = Pl/Es

This index has a range from 1 to ∞ usually less than 100. This index shows how the plan length differs from the extension of the cave, this difference is related to the presence of branches or to high sinuosity index of the cave (Piccini, 2011). Lava tubes are not so sinuous and for this reason, this index can be useful to subdivide single tubes from branched tubes.

Horizontality index *(Hi)* = Pl/Lr

Ranges from 1 to zero, lava tubes with high Hi have an almost perfect horizontal pattern, which is common for lava tube patterns (Piccini, 2011).

Linearity index *(Li)* = (Es2 – Vr2) ½ / Lr

It theoretically ranges from 1 to zero and indicates how much a cave has a pattern that fits a straight line, either vertical, inclined, or horizontal (Piccini, 2011).

Dimensional Parameters and morphometrics indices	Acronym	Source
Vertical range	Vr (m)	-Total range from the highest to the lower point of the cave
Real length	Lr (m)	-Total length of the cave, considering all the passages the slope and the vertical sections
Area of long. Section	As (m^2)	-Total area measured on the longitudinal section
Area of plan map	Ap (m^2)	-Total area measured on the plan map
Perimeter of plan map	Pp (m)	-Perimeter of the plan map
Area over Perimeter	*Ap/Pp	- Is the area of plan map over perimeter of plan map
Plan length	Pl (m)	-Totale length of all the branches measured on the plan map
Extension (long axis)	Es (m)	-Distance between the two farthest points of the cave
Short Axis	S (m)	-Measured on the short axis of the minimum oriented rectangle
Short axis over Extension	*S/Es	S/Es is the ratio between short axis (S) over long axis (Es)
Horizontal complexity index	*Hci	-Lp/Es, range from 1 to ∞ usually less than 100
Horizontality index	*Hi	-Lp/Lr, ranges from 1 to zero
Vertical Index	*Vi	-Vr/Lr , range from 1 to zero
Linearity index	*Li	-(Es2 – Vr2) ½ / Lr, range from 1 to zero
Average width of cave passage	Wa (m)	-Ap/Lp, the average width of the cave
Cave field	*Cf (m^2)	-Is the area of the minimum oriented rectangle that surround the cave
Box fill	*Bf	-Ap/Cf, is expressed as a percentage
Slope°	Sl	-It is measured on the longitudinal section, taking the farthest points of the cave
Areal Coverage	*[1]Ac	-Ap/Cf the area of the cave itself over the area of the bounding box

Dimensional Parameters and morphometrics indices	Acronym	Source
Average Height	Ha (m)	-As/Lr or As/Ls, Area of the longitudinal section over real length or the length of longitudinal section.
Average Linear Volume	*[1]aLV (m^3)	-[(Ha/2)*(Wa/2)] * π, is the volume per 1 m thick cross-section
Tot. Average Linear Volume	*[1]VtC (m^3)	-aLV*Lr, is the average linear volume multiplied real length
Average Volume of the Cave	*VtC 2 (m^3)	-Ap*Ha, is another way to measure the cave volume
Bounding Box Volume	VBb (m^3)	-Cf*Vr, is the total volume of the bounding box
Average Aspect ratio	Ar	-Wa/Ha, average aspect ratio of cave cross-sections
Cave porosity	*Cp	-VtC/VBb, it is expressed as a percentage
Specific Volume	*Vs	-VtC2/Lr, the average size of the cave passage

*Table 6: Dimensional parameters and morphometrics indices extracted from lava tubes survey. * Parameters and indices from Sauro et al., 2020, *[1] parameters and indices from Piccini, 2011.*

4.3-Lava tubes morphotypes

Some morphological elements of caves are important to discriminate among different morphological typologies in turn, useful to understand the genetic process. First I have quantitatively subdivided the lava tubes into two groups: single and braided. In particular, the braided tubes have been defined when splitting into two or more branches were observed. Even tubes showing a loop pattern in planar view (splitting and reconnection of the conduits) are considered braided. As we will see in the results chapter the quantitative analysis has shown that tubes with loop patterns are not always characterized by indices and parameters typical of braided tubes. An example of braided tube is *Grotta del Santo* on the south-western flank of Mount Etna; it shows several branches that complicate the plan view. A typical single-tube is instead the *Thurston lava tube* (Big Island-Hawaii), which is characterized by the planar map in which the caves develop only along one main gallery. Both single and braided type can show many different morphologies, referring to the evolution of the tube. For instance, they can show multi-levels morphologies along their section. For example, single tube of *la Corona* (Lanzarote- Canary island) shows many sections with 2 or 3 superposed levels, and also the braided-type lava tube *Monte Intraleo cave* (Mt. Etna), is characterized by 2 levels superposed. In addition, in both single and braided tubes, we can observe morphologies such as engraved canyons, similar to canyons formed in karst rocks by water erosion. To better subdivide single-type from braided, I also extrapolated the various dimensional parameters and morphometric indices described in the previous section. The results of this analysis are presented in Chapter 5.

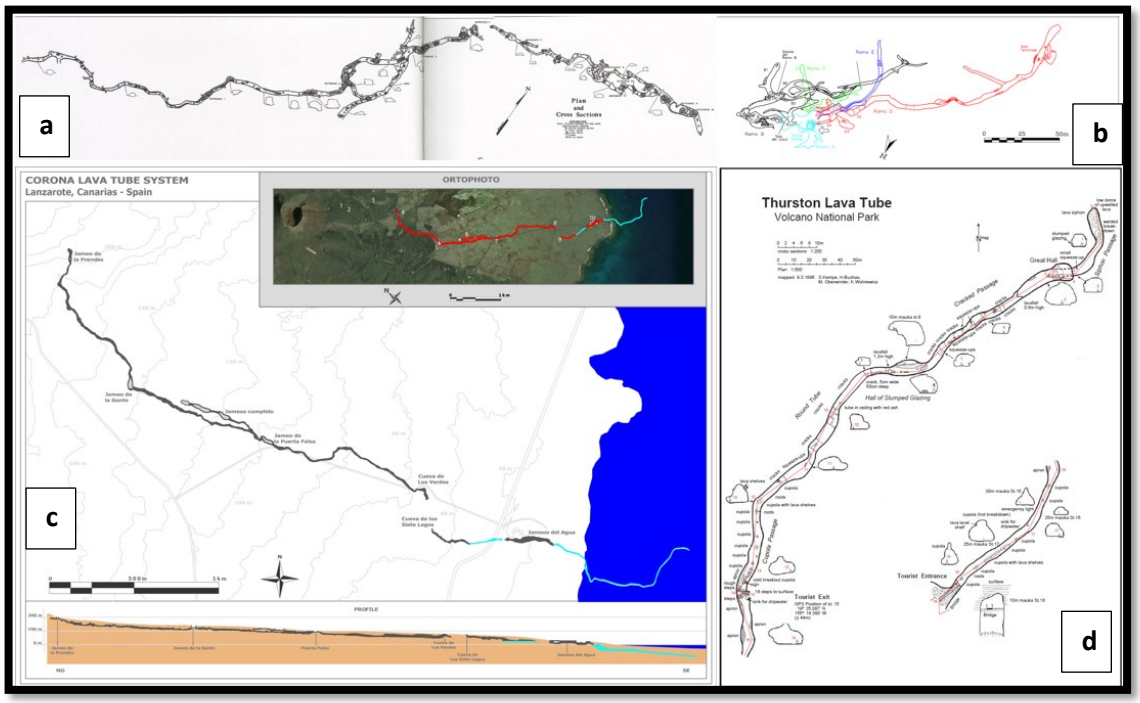

Figure 17: Plan maps of different lava tubes showing the difference between braided (a and b), and single (c and d). a) Surtshellir-Stefanshellir (Iceland) braided and loop tube (Hróarsson B, 2006); b) Santo's Cave (Mt. Etna) plan map (Bonaccorso and Santi, 1999); c) la Corona lava tube (Lanzarote-Canary Island) single tube (Sauro et al., 2020); d) Thurston Lava Tube (Island of Hawaii-Hawaiian Archipelagos), single tube (Kempe & Henschel, 2008).

5-Results:

In this chapter, I will introduce the results obtained by digitizing the surveys and comparing the parameters seen in the previous chapter.

5.1-Parameters and indices

For this work, 36 lava tube surveys were digitalized, from which 27-dimensional parameters and morphometric indices were extracted and derived (see Table 8). All the parameters and indices extracted were compared with parameters already known, such as the ones of La Corona lava tube (Lanzarote-Canary Island). Indeed, the main path of the entire La Corona cave system was mapped with an unprecedented resolution of a few centimeters, the result is one of the longest 3-D surveys of terrestrial lava tubes to date (Santagata et al., 2018; Sauro et al., 2019; Sauro et al., 2020). Through this high-resolution survey, several data have been extrapolated, such as the real length the average interior width, and the average interior height of the conduits (Sauro et al., 2020). These data were compared with those obtained by digitizing the 2-D survey of the La Corona lava tube, to prove the reliability of the method adopted in the present thesis. In Table 7 we compared the data from Sauro et al., (2020) with the results of digitalization work, finding a good match between the results of the two methods and thus, confirming the good reliability of the adopted methodology.

Lava Tube	Ha (m)	Wa (m)	*[1] aLV(m^3)	* Vs (m^3)
La Corona 2D	10.08	14.36	113.64	87.40
*[1]La Corona 3D	9.7	13.7	104	–

*Table 7: Results from Sauro et al. (2020) morphometrics extraction compared with morphometrics parameters and indices extracted in this work, the example of La Corona Lava Tube (Lanzarote- Canary Island). * Parameters and indices from Piccini, 2011; *[1] parameters and indices from Sauro et al., 2020.*

Lava Tube	Morphotype	Vr (m)	Lr (m)	As (m²)	Ap (m²)	Pp (m)	Pl (m)
Nuovalucello 1 (Et)	Braided	16.00	266.00	0.00	818.00	445.00	246.00
Grotta Dei Tedeschi (Et)	Braided	5.00	345.00	379.00	1926.00	597.00	290.00
Micio Conti (Et)	Braided	10.00	323.00	0.00	1699.00	493.00	313.00
Grotta Cutrona (Et)	Braided	97.00	872.00	3068.00	4419.00	1707.00	822.00
Maguez (L)	Braided	21.00	974.00	343.00	2577.00	1202.00	786.00
Naturalistas (L)	Braided	17.00	1680.00	3574.80	13973.00	2579.00	1598.00
Manu Nui cave system (H)	Braided	347.00	3490.00	1457.00	3619.00	2595.00	1617.00
Immacolatella 1 (Et)	Braided	10.00	325.00	0.00	3708.00	716.00	287.00
Surthshellir-Stefanshellir (I)	Braided	30.00	3490.00	21385	25840.00	4686.00	2902.00
Grotta Dei Lamponi (Et)	Braided	93.00	720.00	2326.00	3121.00	1120.00	679.00
Terraced cave (H)	Braided	29.00	434.00	1869.00	3239.00	899.00	434.00
Tusk cave (H)	Braided	15.00	197.00	528.00	1437.00	311.00	171.00
Kuamo'o Point Sea Cave (H)	Braided	8.00	154.00	328.00	719.00	316.00	154.00
Grotta del Santo (Et)	Braided ML	44.00	924.00	824.00	2119.00	1350.00	861.00
Cueva di Elena (Et)	Braided ML	55.00	677.00	2255.00	2678.00	1289.00	643.00
Grotta Monte Intraleo (Et)	Braided ML	16.00	317.00	762.00	1394.00	626.00	298.00
Las Breñas (L)	Braided ML	42.00	2269.00	3917.00	6421.00	3662.00	2114.00
Grotta Corsaro (Et)	Single	130.00	367.00	1055.00	1539.00	715.00	341.00
Catanese1 (Et)	Single	27.00	180.00	588.00	763.00	297.00	153.00

MA.RA.SCA (Et)	Single	154.00	641.00	1656.00	2781.00	1238.00	608.00
Grotta del Burrò (Et)	Single	47.00	297.00	1452.00	1962.00	558.00	245.00
Grotta del Gelo (Et)	Single	30.00	167.00	716.00	851.00	249.00	115.00
Grotta del Diavolo (Et)	Single	61.00	295.00	1342.00	1491.00	536.00	261.00
Hana Gardenland Cave (H)	Single	10.00	209.00	519.00	1528.00	398.00	173.00
Lying Eyes Cave (H)	Single	9.00	58.00	125.00	442.00	134.00	52.00
Sweet Sunday Caves (H)	Single	43.00	404.00	1385.00	2296.00	752.00	361.00
Thurston Lava Tube (H)	Single	20.00	531.00	1669.00	3159.00	1114.00	490.00
Buri Cave (I)	Single	45.00	1025.00	5383.00	9260.00	1966.00	946.00
Viðgelmir Cave (I)	Single	36.00	1584.00	11982.00	16249.00	2994.00	1466.00
Tom's Hole (H)	Single	100.00	121.00	388.00	491.00	216.00	105.00
Salto Della Giumenta (Et)	Single	74.00	322.00	997.00	877.00	518.00	212.00
Hammer Cave (H)	Single ML	25.00	252.00	734.00	1034.00	441.00	222.00
Trelivelli-KTM (Et)	Single ML	404.00	1793.00	5761.00	6451.00	3001.00	1481.00
Cueva de Kastdalen (G)	Single ML	73.00	1857.00	6164.00	5223.00	2325.00	1141.00
Grotta Degli Archi (Et)	Single ML	73.00	555.00	0.00	2955.00	706.00	342.00
La Corona (L)	Single ML	374.00	8960.00	46368.00	77710.00	11273.00	5410.00

Lava Tube	**Morphotype**	***Hci**	***Hi**	***Vi**	***Li**	**Ar**	***Cp**
Nuovalucello 1 (Et)	Braided	1.64	0.92	0.06	0.56	0.00	0%
Grotta Dei Tedeschi (Et)	Braided	2.23	0.84	0.01	0.38	6.05	11%
Micio Conti (Et)	Braided	1.75	0.97	0.03	0.55	0.00	0%
Grotta Cutrona (Et)	Braided	1.98	0.94	0.11	0.46	1.53	0%

Maguez (L)	Braided	2.61	0.81	0.02	0.31	2.87	1%
Naturalistas (L)	Braided	1.70	0.95	0.01	0.56	4.11	2%
Manu Nui cave system (H)	Braided	2.48	0.46	0.10	0.16	0.98	0%
Immacolatella 1 (Et)	Braided	1.47	0.88	0.03	0.60	0.00	0%
Surthshellir-Stefanshellir (I)	Braided	1.77	0.83	0.01	0.47	1.45	2%
Grotta Dei Lamponi (Et)	Braided	1.53	0.94	0.13	0.60	1.42	0%
Terraced cave (H)	Braided	1.49	1.00	0.07	0.67	1.73	5%
Tusk cave (H)	Braided	1.49	0.87	0.08	0.58	3.14	12%
Kuamo'o Point Sea Cave (H)	Braided	1.48	1.00	0.05	0.67	2.19	9%
Grotta del Santo (Et)	Braided ML	3.95	0.93	0.05	0.23	2.76	1%
Cueva di Elena (G)	Braided ML	1.89	0.95	0.08	0.50	0.89	2%
Grotta Monte Intraleo (Et)	Braided ML	2.04	0.94	0.05	0.46	1.95	4%
Las Breñas (L)	Braided ML	3.62	0.93	0.02	0.26	1.76	0%
Grotta Corsaro (Et)	Single	1.02	0.93	0.35	0.84	1.57	1%
Catanese1 (Et)	Single	1.06	0.85	0.15	0.79	1.53	8%
MA.RA.SCA (Et)	Single	1.07	0.95	0.24	0.85	1.77	0%
Grotta del Burrò (Et)	Single	1.05	0.82	0.16	0.77	1.64	4%
Grotta del Gelo (Et)	Single	1.10	0.69	0.18	0.60	1.73	8%
Grotta del Diavolo (Et)	Single	1.15	0.88	0.21	0.74	1.26	2%
Hana Gardenland Cave (H)	Single	1.28	0.83	0.05	0.64	3.56	16%
Lying Eyes Cave (H)	Single	1.02	0.90	0.16	0.87	3.94	30%
Sweet Sunday Caves (H)	Single	1.06	0.89	0.11	0.83	1.86	3%

Thurston Lava Tube (H)	Single	1.13	0.92	0.04	0.81	2.05	3%
Buri Cave (I)	Single	1.12	0.92	0.04	0.82	1.86	3%
Viðgelmir Cave (I)	Single	1.16	0.93	0.02	0.80	1.47	3%
Tom's Hole (H)	Single	1.13	0.87	0.83	0.00	1.46	3%
Salto Della Giumenta (Et)	Single	1.04	0.66	0.23	0.59	1.34	1%
Hammer Cave (H)	Single ML	1.14	0.88	0.10	0.76	1.60	5%
Trelivelli-KTM (Et)	Single ML	1.09	0.83	0.23	0.72	1.36	0%
Cueva de Kastdalen (G)	Single ML	1.08	0.61	0.04	0.57	1.05	1%
Grotta Degli Archi (Et)	Single ML	1.06	0.62	0.13	0.57	0.00	0%
La Corona (L)	Single ML	1.33	0.60	0.04	0.45	1.43	0%

Lava Tube	**Morphotype**	**Wa (m)**	***Cf (m²)**	**Sl**	**Ha (m)**	**Es (m)**	**S(m)**
Nuovalucello 1 (Et)	Braided	3.33	4948.00	6.00	0.00	150.00	32.99
Grotta dei Tedeschi (Et)	Braided	6.64	7386.00	1.00	1.10	130.00	56.82
Micio Conti (Et)	Braided	5.43	6962.00	0.00	0.00	179.00	38.89
Grotta Cutrona (Et)	Braided	5.38	98011.00	13.00	3.52	416.00	235.60
Maguez (L)	Braided	3.28	26698.00	5.00	1.14	301.00	88.70
Naturalistas (L)	Braided	8.74	148195.00	1.00	2.13	941.00	157.49
Manu Nui Cave System (H)	Braided	2.24	46576.00	15.00	2.27	653.00	71.33
Immacolatella 1 (Et)	Braided	12.92	11210.00	0.00	0.00	195.00	57.49
Surthshellir-Stefanshellir (I)	Braided	8.90	400172.00	1.00	6.13	1636.00	244.60

Grotta Dei Lamponi (Et)	Braided	4.60	52030.00	10.00	3.23	445.00	116.92
Terraced Cave (H)	Braided	7.46	14045.00	4.00	4.31	292.00	48.10
Tusk Cave (H)	Braided	8.40	3965.00	6.00	2.68	115.00	34.48
Kuamo'o Point Sea Cave (H)	Braided	4.67	3237.00	4.00	2.13	104.00	31.13
Grotta del Santo (Et)	Braided ML	2.46	14108.00	9.00	0.89	218.00	64.72
Cueva di Elena (G)	Braided ML	4.16	22540.00	5.00	4.66	341.00	66.10
Grotta Monte Intraleo (Et)	Braided ML	4.68	7846.00	5.00	2.40	146.00	53.74
las Breñas (L)	Braided ML	3.04	128000.00	4.00	1.73	584.00	219.18
Grotta Corsaro (Et)	Single	4.51	10916.00	19.00	2.87	334.00	32.68
Catanese1 (Et)	Single	4.99	2129.00	13.50	3.27	145.00	14.68
MA.RA.SCA (Et)	Single	4.57	41860.00	14.00	2.58	569.00	73.57
Grotta del Burrò (Et)	Single	8.01	9675.00	11.00	4.89	233.00	41.52
Grotta del Gelo (Et)	Single	7.40	3277.00	15.00	4.29	105.00	31.21
Grotta del Diavolo (Et)	Single	5.71	9309.00	12.00	4.55	227.00	41.01
Hana Gardenland Cave (H)	Single	8.83	4412.00	5.00	2.48	135.00	32.68
Lying Eyes Cave (H)	Single	8.50	617.00	8.00	2.16	51.00	12.10
Sweet Sunday Caves (H)	Single	6.36	10590.00	7.00	3.43	340.00	31.15
Thurston Lava Tube (H)	Single	6.45	26514.00	2.00	3.14	432.00	61.38
Buri Cave (I)	Single	9.79	68457.00	1.00	5.25	844.00	81.11
Viðgelmir Cave (I)	Single	11.08	187876.00	1.00	7.56	1269.00	148.05
Tom's Hole (H)	Single	4.68	1065.00	14.00	3.21	93.00	11.45
Salto della Giumenta (Et)	Single	4.14	7326.00	18.00	3.10	204.00	35.91

Hammer Cave (H)	Single ML	4.66	4371.00	8.00	2.91	194.00	22.53
Trelivelli-KTM (Et)	Single ML	4.36	348850.21	13.50	3.21	1357.00	257.07
Cueva de Kastdalen (G)	Single ML	4.58	154610.00	4.00	4.37	1057.00	146.27
Grotta degli Archi (Et)	Single ML	8.64	14596.00	12.00	0.00	323.00	45.19
La Corona (L)	Single ML	14.36	2565845.00	3.00	10.08	4077.00	629.35

Lava Tube	**Morphotype**	***¹aLV(m³)**	***¹VtC (m³)**	***VtC 2 (m³)**	**VBb (m³)**	***Vs (m³)**
Nuovalucello 1 (Et)	Braided	0.00	0.00	0.00	79168.00	0.00
Grotta dei Tedeschi (Et)	Braided	11.45	3951.82	2115.81	36930.00	2.05
Micio Conti (Et)	Braided	0.00	0.00	0.00	69620.00	6.13
Grotta Cutrona (Et)	Braided	29.70	25894.48	15547.58	9507067.00	0.00
Maguez (L)	Braided	5.88	5727.14	2943.75	560658.00	17.83
Naturalistas (L)	Braided	29.21	49075.45	29732.55	2519315.00	4.89
Manu Nui Cave System (H)	Braided	7.99	27876.99	8226.80	16161872.00	3.02
Immacolatella 1 (Et)	Braided	0.00	0.00	0.00	112100.00	17.70
Surthshellir-Stefanshellir (I)	Braided	85.66	298953.75	158334.79	12005160.00	2.36
Grotta dei Lamponi (Et)	Braided	23.31	16785.46	10082.56	4838790.00	18.43
Terraced Cave (H)	Braided	50.46	21899.30	13948.60	407305.00	45.37
Tusk Cave (H)	Braided	35.36	6966.17	3851.45	59475.00	14.00
Kuamo'o Point Sea Cave (H)	Braided	15.61	2404.26	1531.38	25896.00	32.14
Grotta del Santo (Et)	Braided ML	3.45	3183.87	1889.67	620752.00	19.55
Cueva di Elena (G)	Braided ML	30.46	20624.77	12477.05	1239700.00	9.94
Grotta Monte Intraleo (Et)	Braided ML	17.65	5596.30	3350.88	125536.00	10.57

las Breñas (L)	Braided ML	8.23	18678.88	11084.64	5376000.00	0.00
Grotta Corsaro (Et)	Single	20.37	7475.43	4424.10	1419080.00	12.05
Catanese1 (Et)	Single	25.58	4603.73	2492.47	57483.00	13.85
MA.RA.SCA (Et)	Single	18.55	11892.07	7184.61	6446440.00	11.21
Grotta del Burrò (Et)	Single	61.47	18255.73	9592.00	454725.00	32.30
Grotta del Gelo (Et)	Single	49.81	8318.49	3648.60	98310.00	21.85
Grotta del Diavolo (Et)	Single	40.80	12036.20	6782.79	567849.00	22.99
Hana Gardenland Cave (H)	Single	34.43	7196.88	3794.41	44120.00	18.16
Lying Eyes Cave (H)	Single	28.76	1668.13	952.59	5553.00	16.42
Sweet Sunday Caves (H)	Single	34.23	13829.74	7871.19	455370.00	19.48
Thurston Lava Tube (H)	Single	31.81	16893.11	9929.14	530280.00	18.70
Buri Cave (I)	Single	80.71	82726.35	48630.81	3080565.00	47.44
Viðgelmir Cave (I)	Single	131.63	208507.48	122913.84	6763536.00	77.60
Tom's Hole (H)	Single	23.54	2848.55	1574.45	106500.00	13.01
Salto della Giumenta (Et)	Single	20.11	6475.28	2715.43	542124.00	8.43
Hammer Cave (H)	Single ML	21.30	5367.39	3011.73	109275.00	11.95
Trelivelli-KTM (Et)	Single ML	21.97	39397.58	20727.39	140935485.75	11.56
Cueva de Kastdalen (G)	Single ML	31.44	58384.50	22849.23	11286530.00	12.30
Grotta degli Archi (Et)	Single ML	0.00	0.00	0.00	1065508.00	0.00
La Corona (L)	Single ML	113.64	1018177.37	783146.55	959626030.00	87.40
Lava Tube	**Morphotype**	**Ap/Es**	***[1]Ac**	***Bf**	***Ap/Pp**	
Nuovalucello 1 (Et)	Braided	5.45	0.17	17%	1.84	

Grotta dei Tedeschi (Et)	Braided	9.72	0.26	15%	1.57
Micio Conti (Et)	Braided	14.82	0.24	26%	3.23
Grotta Cutrona (Et)	Braided	9.49	0.05	24%	3.45
Maguez (L)	Braided	10.62	0.10	5%	2.59
Naturalistas (L)	Braided	10.99	0.09	5%	1.75
Manu Nui Cave System (H)	Braided	8.56	0.08	10%	2.14
Immacolatella 1 (Et)	Braided	14.85	0.33	9%	5.42
Surthshellir-Stefanshellir (I)	Braided	5.54	0.06	8%	1.39
Grotta dei Lamponi (Et)	Braided	7.85	0.06	12%	2.08
Terraced Cave (H)	Braided	15.79	0.23	6%	5.51
Tusk Cave (H)	Braided	7.01	0.36	6%	2.79
Kuamo'o Point Sea Cave (H)	Braided	11.09	0.22	23%	3.60
Grotta del Santo (Et)	Braided ML	12.50	0.15	36%	4.62
Cueva di Elena (G)	Braided ML	6.91	0.12	22%	2.28
Grotta Monte Intraleo (Et)	Braided ML	9.55	0.18	18%	2.23
las Breñas (L)	Braided ML	19.02	0.05	33%	5.18
Grotta Corsaro (Et)	Single	4.61	0.14	14%	2.15
Catanese1 (Et)	Single	5.26	0.36	36%	2.57
MA.RA.SCA (Et)	Single	4.89	0.07	7%	2.25
Grotta del Burrò (Et)	Single	8.42	0.20	20%	3.52

Grotta del Gelo (Et)	Single	8.10	0.26	26%	3.42
Grotta del Diavolo (Et)	Single	6.57	0.16	16%	2.78
Hana Gardenland Cave (H)	Single	11.32	0.35	35%	3.84
Lying Eyes Cave (H)	Single	8.67	0.72	72%	3.30
Sweet Sunday Caves (H)	Single	6.75	0.22	22%	3.05
Thurston Lava Tube (H)	Single	7.31	0.12	12%	2.84
Buri Cave (I)	Single	10.97	0.14	14%	4.71
Viðgelmir Cave (I)	Single	12.80	0.09	9%	5.43
Tom's Hole (H)	Single	5.28	0.46	46%	2.27
Salto Della Giumenta (Et)	Single	4.30	0.12	12%	1.69
Hammer Cave (H)	Single ML	5.33	0.24	24%	2.34
Trelivelli-KTM (Et)	Single ML	4.75	0.02	2%	4.40
Cueva de Kastdalen (G)	Single ML	4.94	0.03	3%	2.25
Grotta Degli Archi (Et)	Single ML	9.15	0.20	20%	4.19
La Corona (L)	Single ML	19.06	0.03	3%	6.89

*Table 8: Dimensional Parameters and Morphometric indices extracted by digitalization of lava tubes surveys. The lava tubes are subdivided by morphotype: Braided =Braided-type; Single= Single-type; Braided ML= Braided-type with Multi-level structures; Single ML= single-type with Multi-level structures (Multi-level structure, were observed on cave surveys); acronyms for lava tube locations Et = Mt. Etna; H= Hawaii; G=Galapagos; L=Lanzarote; I= Iceland). * Parameters and indices from Piccini, 2011; *[1] parameters and indices from Sauro et al., 2020. The zero values for some parameters or indices are due to the absence of longitudinal sections required to extract them (see Chapter 4.2).*

5.2-Lava tubes Morphotype

In this section, a quantitative classification between single and braided tubes is attempted. In particular, the qualitative distinction described in section 3.4 was compared with the quantitative results. In addition, dimensional parameters and morphometric indices were compared one to each other to highlight possible correlations. Figure 18 show the diagram between plan length (Pl) and extension (Es), with a correlation among all the data described by the intercept line (blue line) with an R^2=0.9348. This line defines the boundary between single-type and braided-type tubes, with an angular coefficient of 1/Hci (1/1.49= 0,67).

Hence, an Hci ≥ 1.49 indicate braided tube, while lower values are typical of a single pattern. Some of the latter might still show branches, loop patterns, but rather limited of compared to the entire tube development. For this reason, the best index to subdivide braided tubes from single tubes is the Hci, which highlights the lateral development out from the main conduit of the lava tubes. Some tubes fall very near the trendline, with Hci slightly less than 1.49, but they were also considered braided-type due to their patterns and considering some small errors in parameters extrapolation. Therefore, the boundary was identified for values of Hci = 1.49 with a transitional range of (± 0.02).

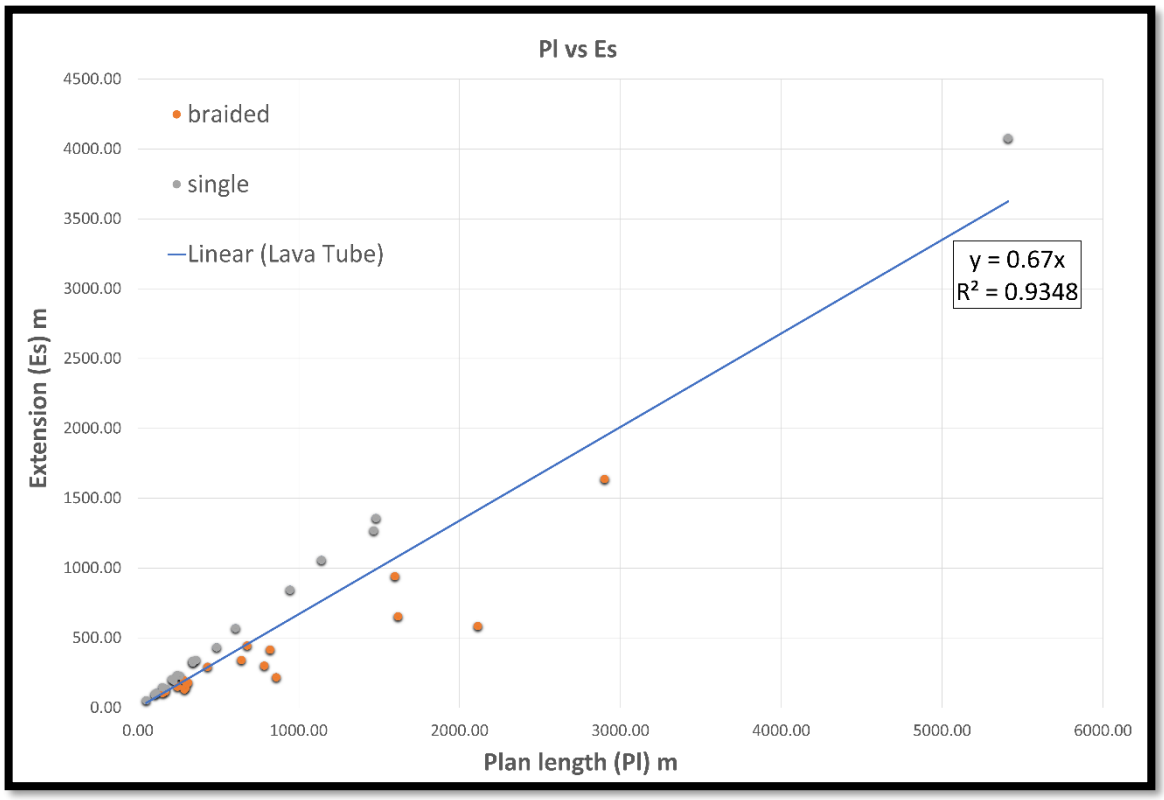

Figure 18: This diagram shows the relation between plan length (Pl) and extension (Es) of the lava tubes, these dimensional parameters are quite perfectly correlated. As the extension increases, the plan length increases, with differences between single and braided types. The blue line is an intercept 0:0 for all the data with an angular coefficient 0.67 is 1/Hci, which outlines the boundary between single and braided type.

In addition, the more complicated is the pattern (i.e., braided tubes) less is the correlation between Pl and Es. Indeed, Pl and Es of single-type tubes are highly correlated following a line defined by the equation $y=0.7597x+66.253$ with an $R^2 = 0.9946$ almost perfectly correlated. Even, single-type ML has a good correlation, between Pl and Es with a $R^2 = 0.9959$, slightly more than single-type tube. However, the limited data ML lava tube do not allow a robust statistic. The Pl and Es braided-type correlation is defined by a $R^2 = 0.8523$, while the braided-type ML show an $R^2 = 0.86$, although still affected by limited data.

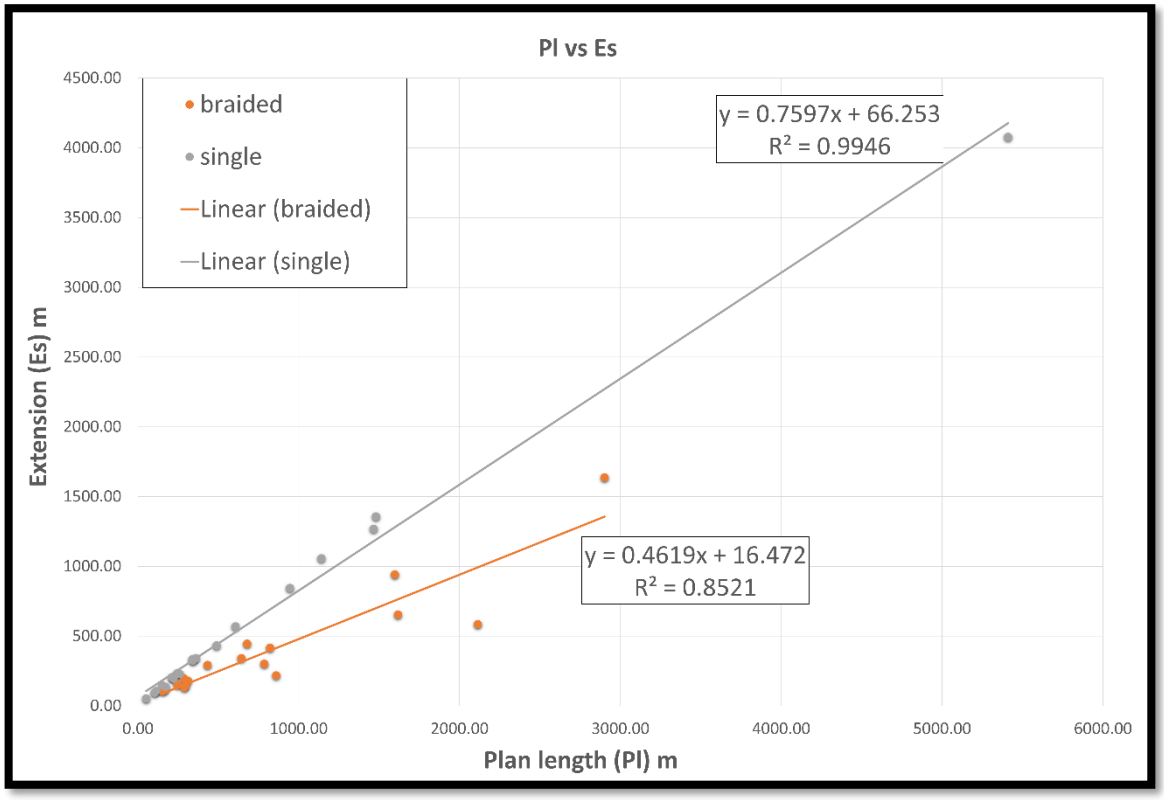

Figure 19: Plan length (Pl) versus the extension (Es) of the lava tubes. The trend lines refer to single and braided categories. The correlation between Pl and Es for single-type tubes is almost perfect, while there is more dispersion for the braided-type data.

Figure 20 shows also the single and braided type with multi-level features, reported respectively as single ML and braided ML.

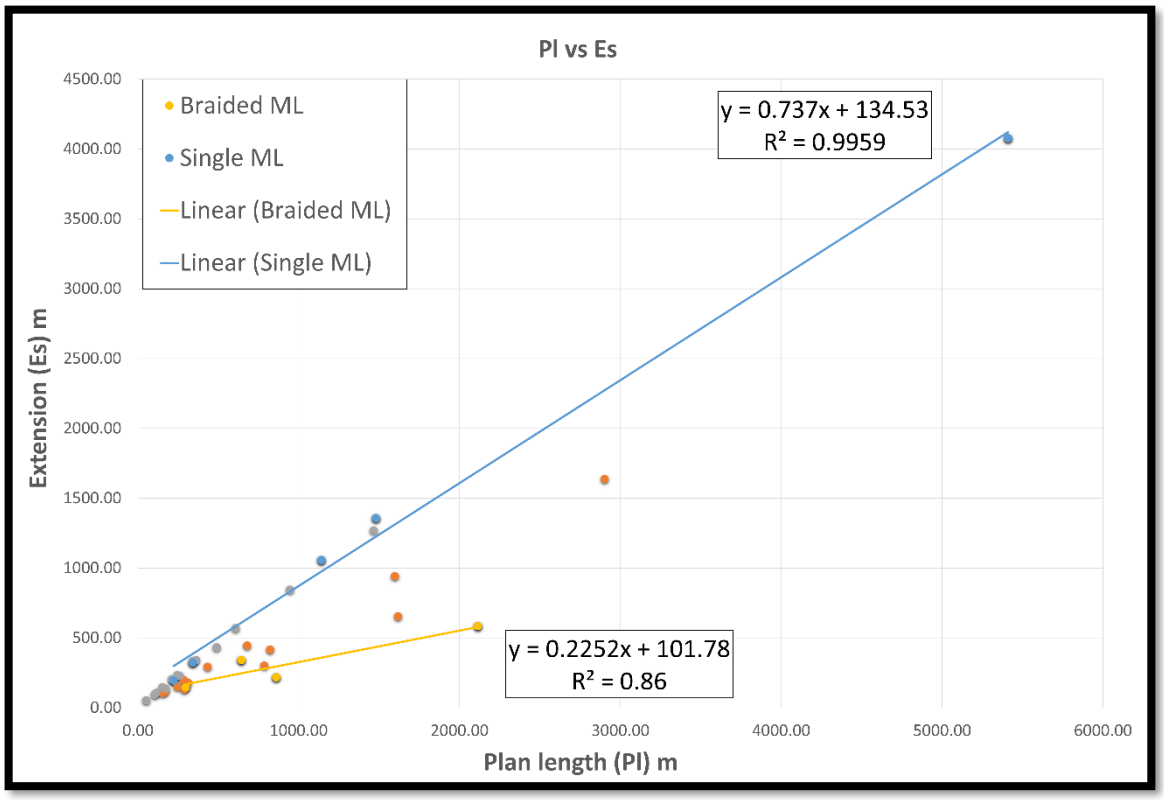

Figure 20: Plan length (Pl) versus extension (Es) of the lava tubes. The trend lines refer to single ML and braided ML categories. The correlation between Pl and Es for of single ML is almost perfect, while there is more dispersion in the braided ML dates. In both cases data are too limited for a robust statistics approach.

5.3- Controlling factors in lava tube development

To understand what leads to the formation of the different categories of lava tubes, I made a diagram of the Horizontal complexity index versus the average slope of each cave. Although the slope is considered one of the main parameters which affect the speleogenesis and evolution of lava tubes I did not find any correlation. Indeed, figure 21 shows how the slope does not impact the cave patterns, or at least not on the whole path. This means that the slope can probably influence the lava tube morphologies only where abrupt changes in slope occur. While Single or Single ML forms at any slope between 0° and 25°, Braided and Braided ML form mainly between 0° and 15° of slope, with only two exceptions documented at over 30°. This clearly shows that slope is only a complementary factor together with effusion rate and viscosity for the formation of single tubes. Instead, the slope range for braided is more limited, showing a more important control in their genesis.

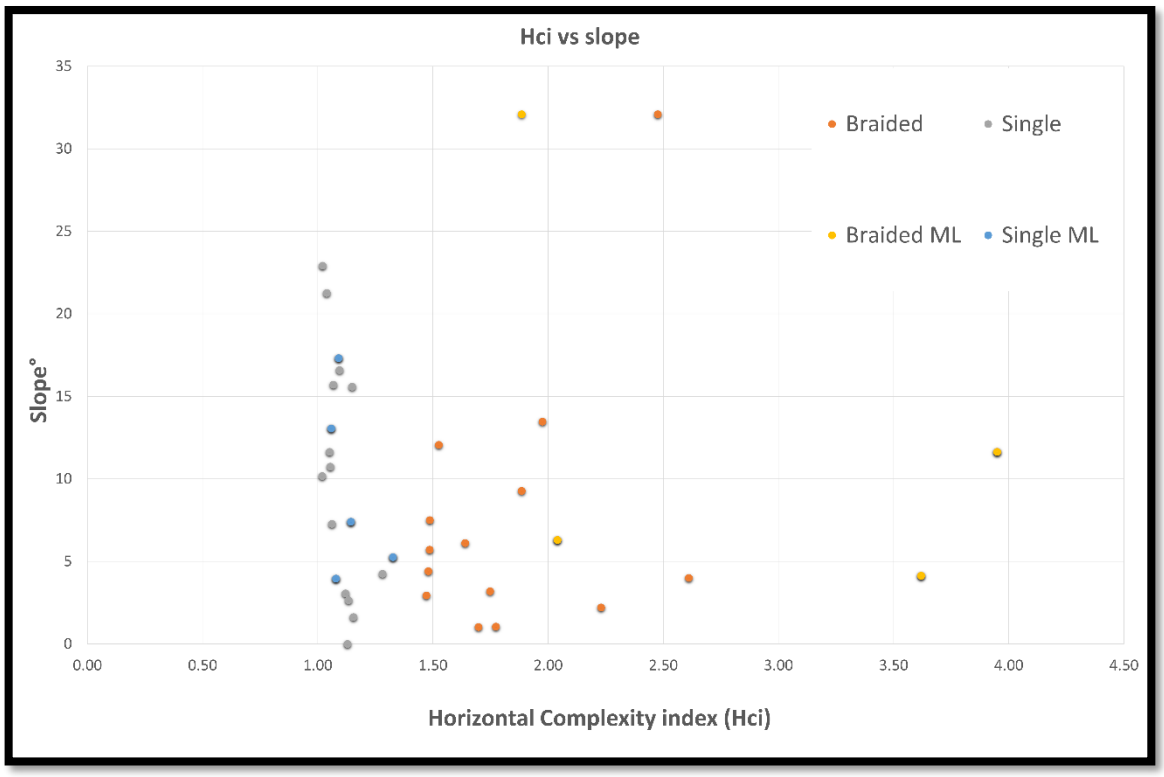

Figure 21: Horizontal complexity index versus the average slope of the lava tubes. Here it's clear that the average slope does not affect the pattern of the lava tubes.

Even the real length (Lr) of the tube does not show any correlation with the average slope (Fig. 22).

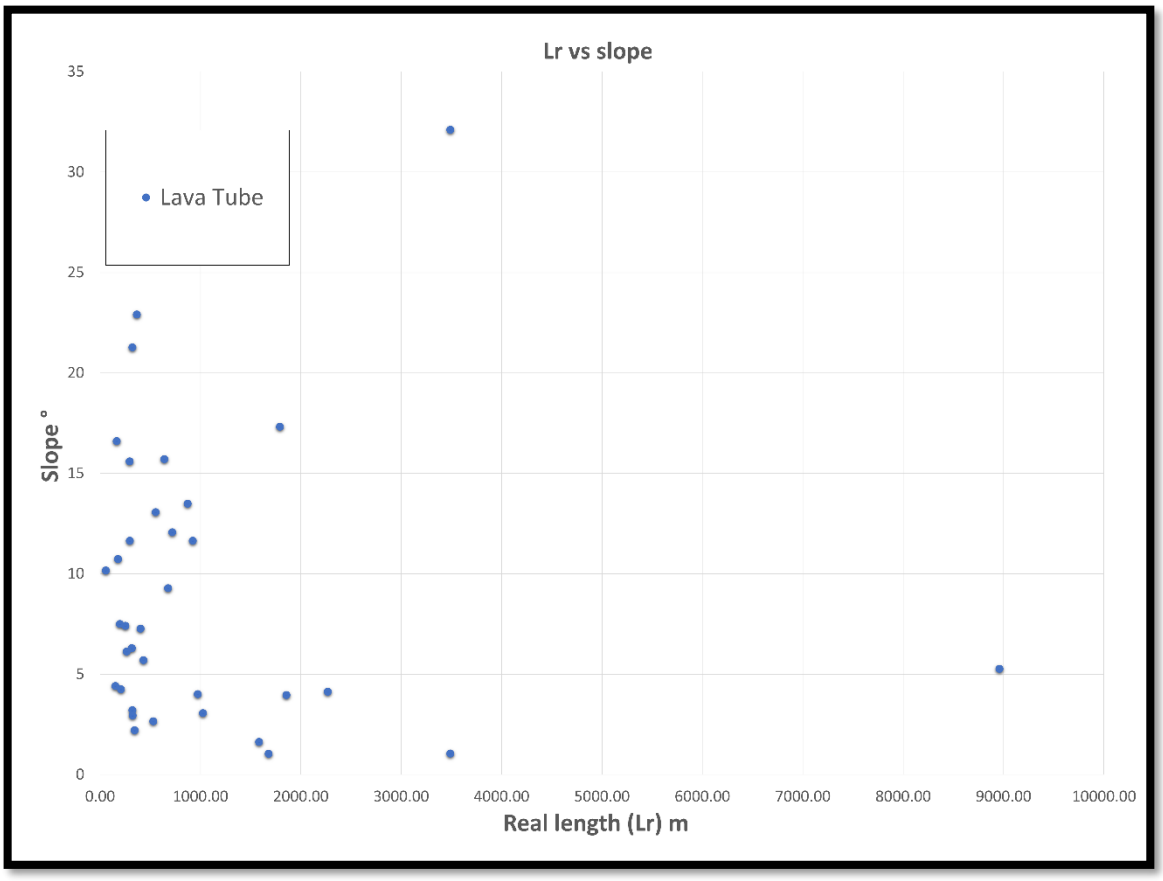

Figure 22: Real length versus average slope. It is clear the absence of any correlation between real length (Lr) and Slope (S).

I have carried out a comparison between dimensional parameters such as real length, extension, and area of the plan map. The diagram's real length (Lr) versus area of the plan map (Ap) shows a meaningful result. Single-type tubes show a good correlation along a best fit linear function with an $R^2 = 0.9682$, while braided-type seems to have more dispersion along a different best fit line with a general low $R^2 = 0.4961$. Single-type has only two data deviating from the trendline, *TreLivelli-KTM* system (Mt. Etna), and *Kastdalen* cave (Santa Cruz Island-Galapagos), as their ratio of Lr to Ap, is low compared with other single-type lava tubes.

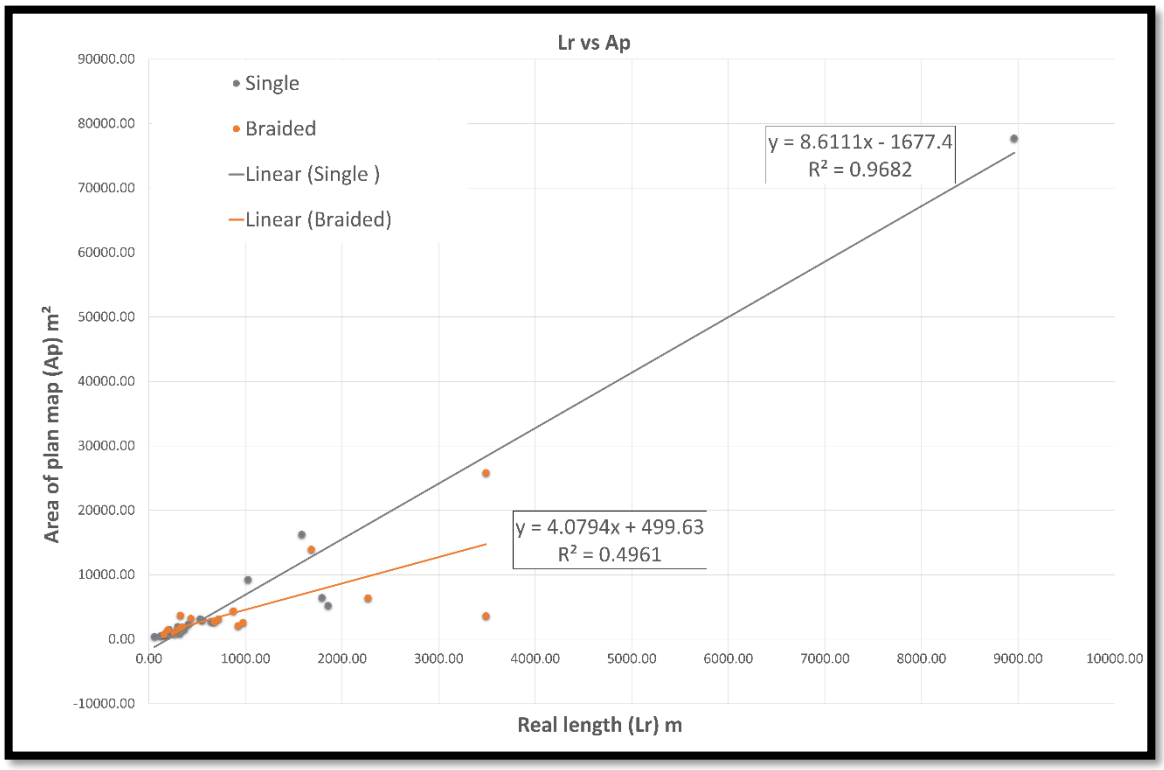

Figure 23: Real length (Lr) versus the plan map area (Ap), where it's reported the trend line for single-type and braided-type. The single-type tubes increasing trend line, defined by the equation y=8.6101x-1668.1 (gray line) has an almost perfect correlation, while braided-type tubes are characterized by a best fit line with the equation y=4.0794x+499.63 (orange line).

Limiting our observation to tubes with a real length lower than 900 meters, the single-type correlation tends to decrease, from an almost perfect correlation $R^2 = 0.9681$ to $R^2 = 0.8423$. regarding braided type after excluding tubes with Lr > 900m., shows an increase in correlation (Fig. 24), this is because braided-type tubes with Lr > 900m. are more dispersed. Indeed, looking at the longest braided-type tubes, Surtshellir-Stefanshellir (Iceland) and Manu Nui cave system (Island of Hawaii) they show the same Lr but a huge difference in Ap (Fig. 23).

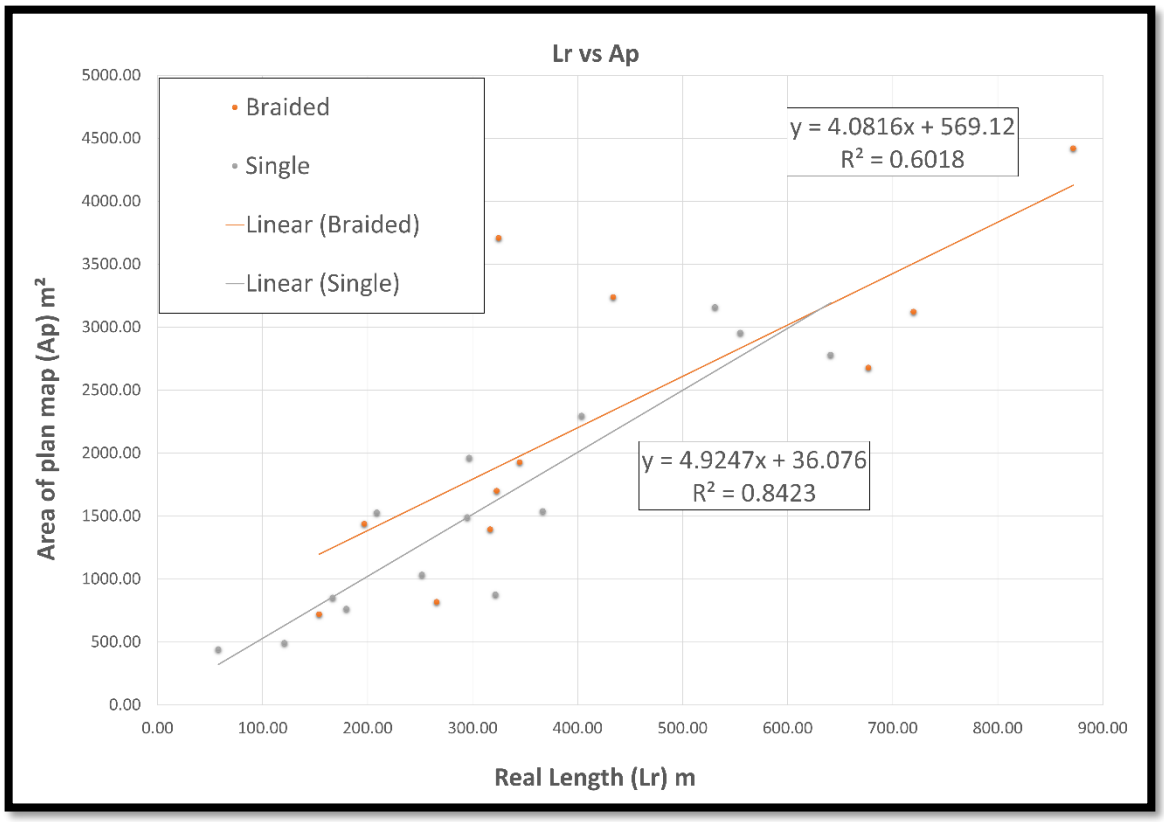

Figure 24: Real length (Lr) versus the area of the plan map (Ap) for tubes with Lr<900 m: in gray the trend line for single-type, in orange the trend line for braided-type. Note the increase of dispersion for single-type and an increase of correlation for braided-type.

Despite the correlation between plan map area and Real Length is good for the single-type lava tube, is not for the braided-type shows a low correlation, so another diagram was developed in order to find a valid parameter for each category. Plotting the extension (Es) versus the area on the planar map (Ap) (Fig. 25). I found a good correlation among all the data along a best fit line with an $R^2 = 0.9161$. In addition, the correlation of braided-type increases significantly from $R^2=0.4961$ in diagram 23 to $R^2 = 0.9248$ (Fig. 25). Concerning single-type we can observe (Fig. 25) a negligible decrease in correlation compared with Figure 23, from $R^2 = 0.9682$ to $R^2 = 0.9208$.

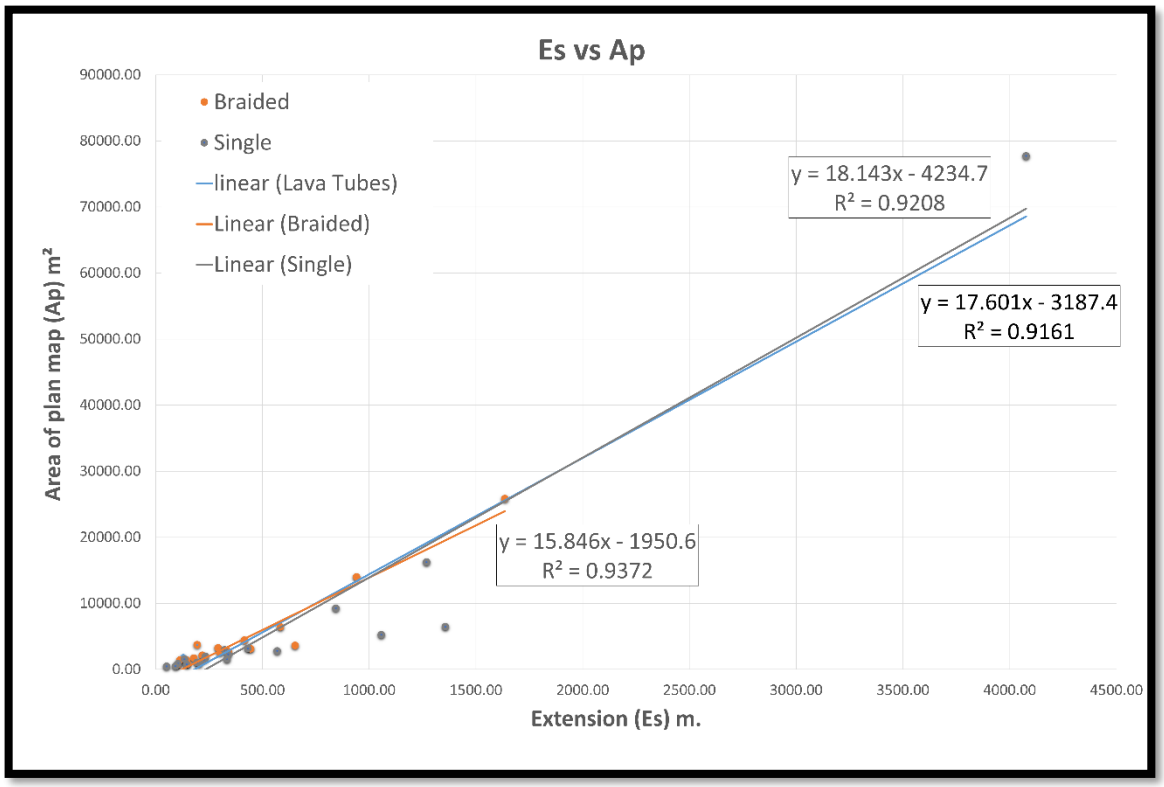

Figure 25: Extension (Es) versus the area of the plan map (Ap), this graph shows the correlation of the single-type (grey line), braided-type (orange line), and all the data (blue line).

To highlight the data in the lower-left zone of the diagram, I have excluded *La Corona* lava tube (Lanzarote-Canary Island), which has much higher values than the rest of the lava tubes. It is observed a decrease of the correlation for all the data and single-type tubes, (La Corona lava tube belongs to these categories). In particular, all the data are characterized by an $R^2 = 0.7534$, while single-type have $R^2 = 0.7078$. No variation of R^2 recorded for braided-type tubes.

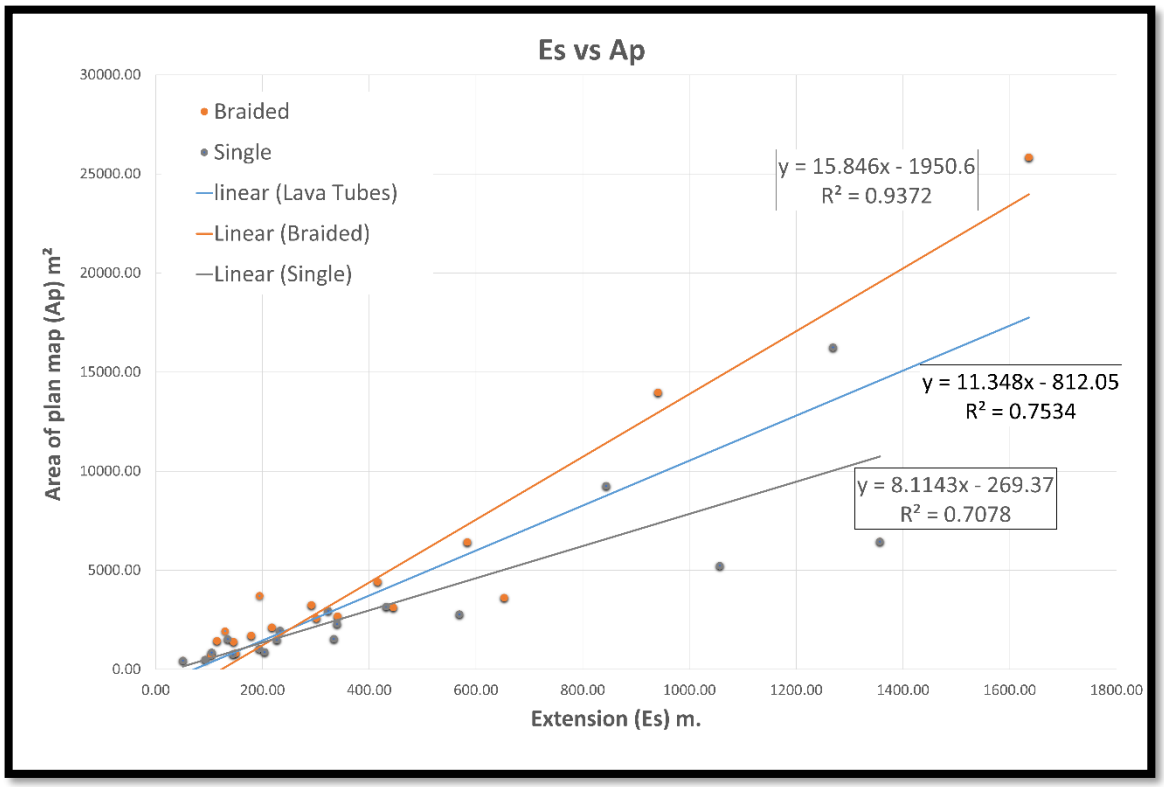

Figure 26: Extension (Es) versus the area of the plan map (Ap), this graph shows the correlation of the single-type without La Corona (grey line), braided-type (orange line), and all the data without La Corona (blue line). Note the decrease in correlation for single-type tubes.

In Figure 26 I have also identified some outliers, which were excluded (Fig. 27-28). The outliers were identified within tubes of smaller extension (Es), that deviate from both of the possible trends identified (Fig. 27-28), one with exponential increase and another with moderate linear increase (Figure 28). Figure 27 reports the category's (single and braided) power curves without outliers, highlighting two different best fit with similar correlations for braided-type ($R^2 = 0.9599$) and single-type ($R^2 = 0.9528$).

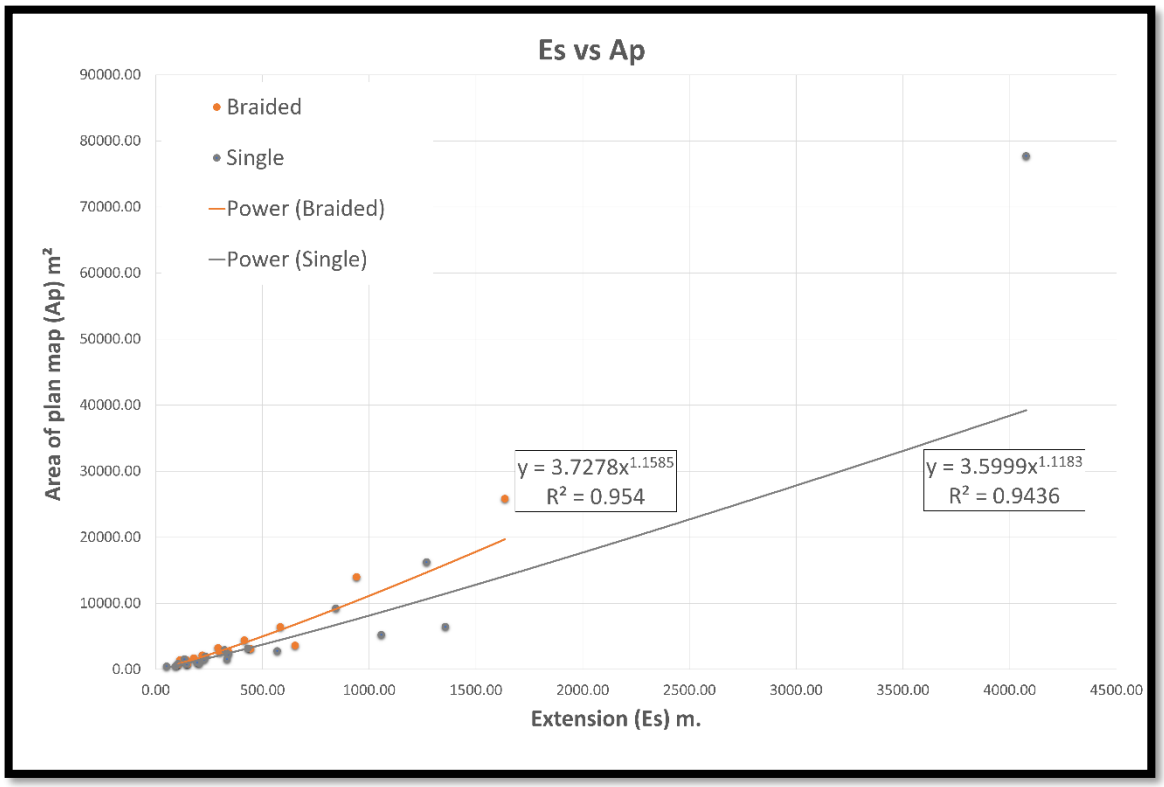

Figure 27: Extension (Es) versus area of plan map (Ap). This diagram shows the power law curve for each category, two outliers have been neglected, Immacolatella 1, and Tedeschi cave (Mt. Etna).

In Figure 28, a power curve fit all data with an $R^2 = 0.9429$ (excluding the above mentioned outliers). This curve evidently identify the boundary between two different trends, below the curve, we have the data associated with a moderate linear increasing trend (brown line), while above the curve the data outlines an exponentially increasing trend (blue line). The exponential increasing trend is described along a power curve defined by the equation $y = 3.7445x^{1.1779}$ with an $R^2 = 0.997$, while a best fit line with the equation $y = 4.7543x+299.04$ with an $R^2=0.941$ (Fig. 28).

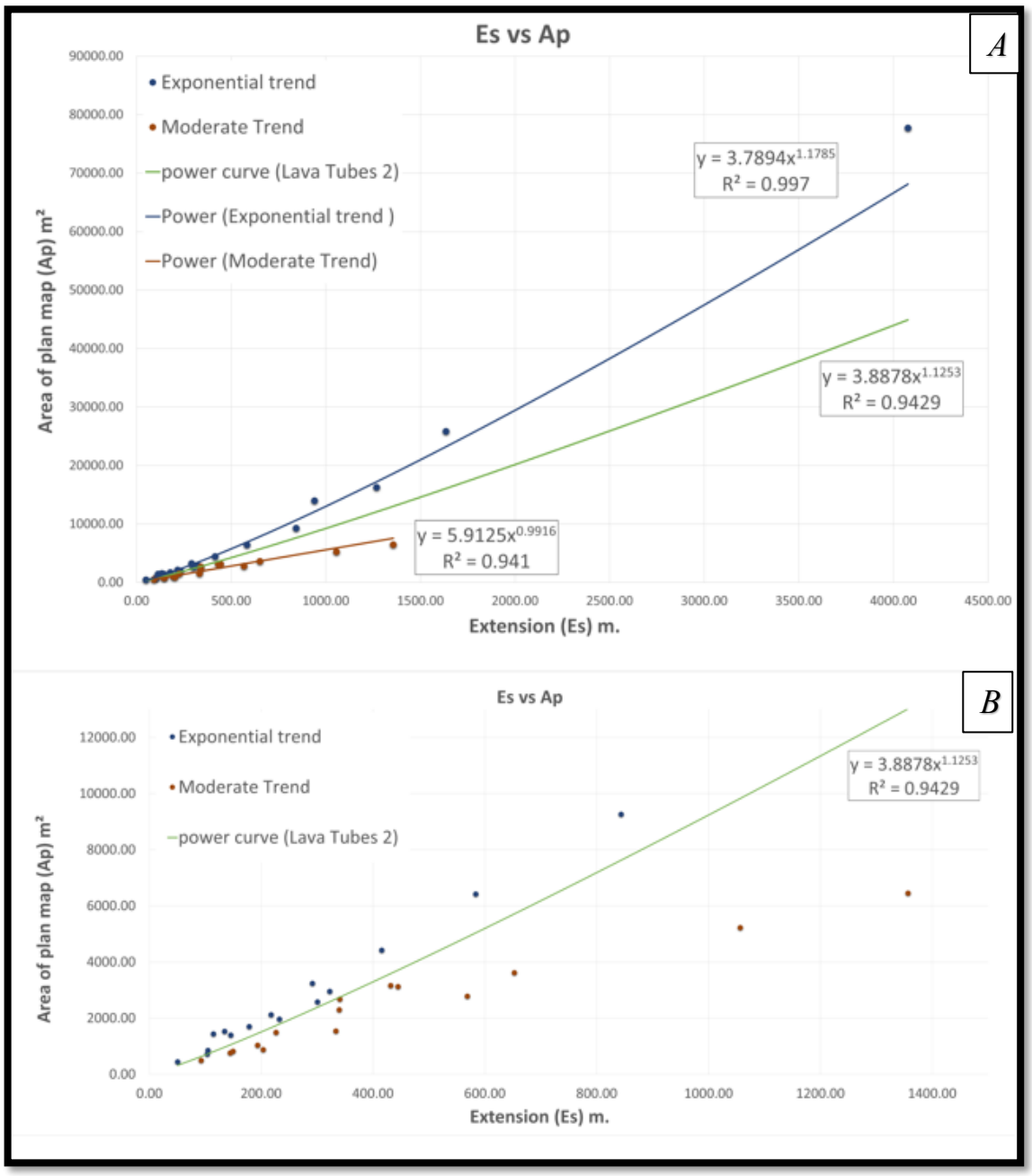

Figure 28: Extension versus area of plan map. A) The moderate increasing trend (brown dots) is characterized by a linear trend with a high correlation (brown line); the exponential increasing trend (blue dots) is defined by a power law curve with an almost perfect correlation (blue line); B) Highlighting the lower zone of the diagram, the green is the power law curve that fit all the data without the outliers, from which two trends, not corresponding to the morphotype (single and braided) of the lava tubes, are recognizable.

The exponential increasing trend is characterized by an exponential increase of the ratio between Ap and Es, while the linear trend shows a moderate increase in this ratio. In Figure 29, I have plotted the data of the Ap/Es against the average aspect ratio (Ar) of each lava tube. Observing the diagram (Fig. 29), is clear that the moderate trend data does not show a great dispersion, indeed the increase of Ar and Ap/Es is contained. Concerning the exponential data the relation between Ar and Ap/Es seems to not follow a rule, indeed with an increase of Ap/Es can be observed both an increase and a decrease of Ar.

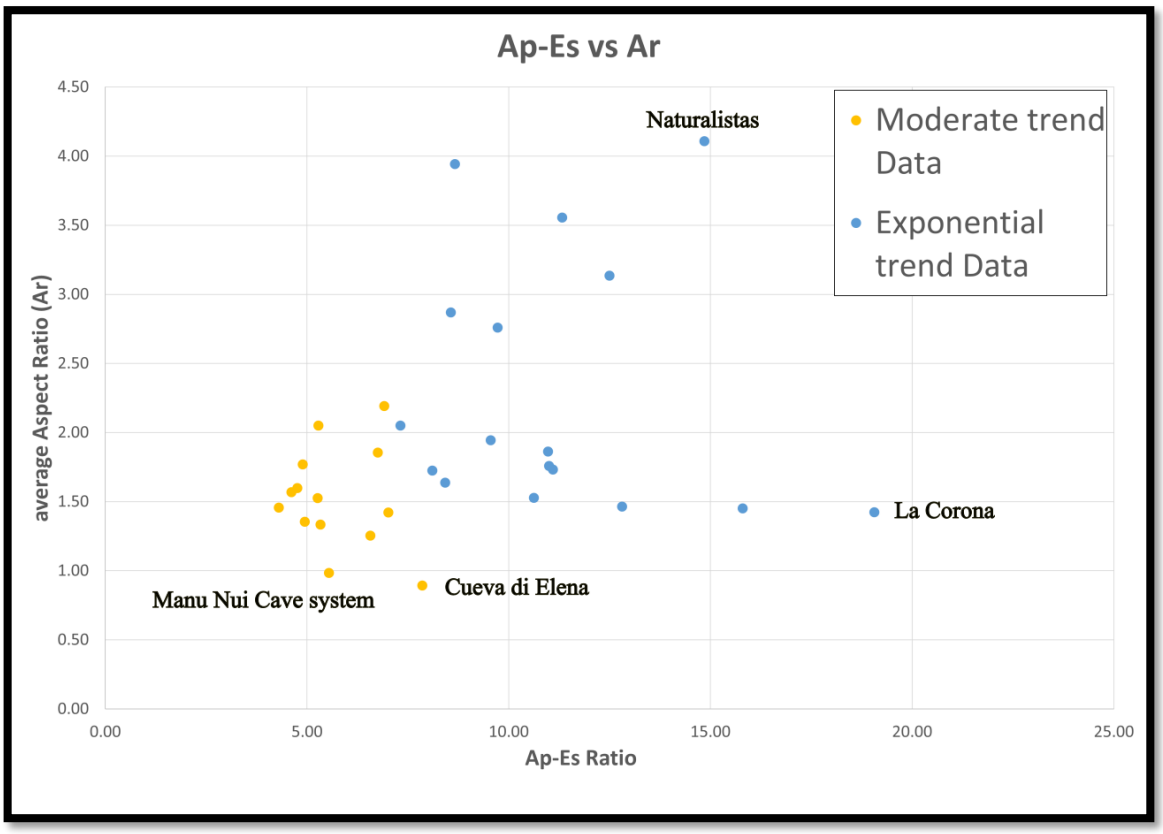

Figure 29: Ap/Es ratio versus the average aspect ratio (Ar). The blue dots are referred to the exponential trend data, while the yellow dots are for the Moderate trend data (see Fig. 28).

As seen, an important characteristic for understanding the possible evolution of a lava tube is the shape of the cross-section, numerically defined by the aspect ratio (Ar). For this reason, I have made some diagrams to determine if a specific dimensional parameter or index (for each of the entire tubes) could be correlated with the average aspect ratio of the lava tubes. A correlation was indeed found (Fig. 30) between the Aspect ratio (Ar) and the vertical range (Vr). More in detail (Vr) appears anticorrelated to the aspect ratio through a power trend line with an $R^2 = 0.5931$. A slightly different power low fit the single-type tubes only with an $R^2=0.5589$, while braided-type tubes follow another power low curve with an $R^2=0.6095$.

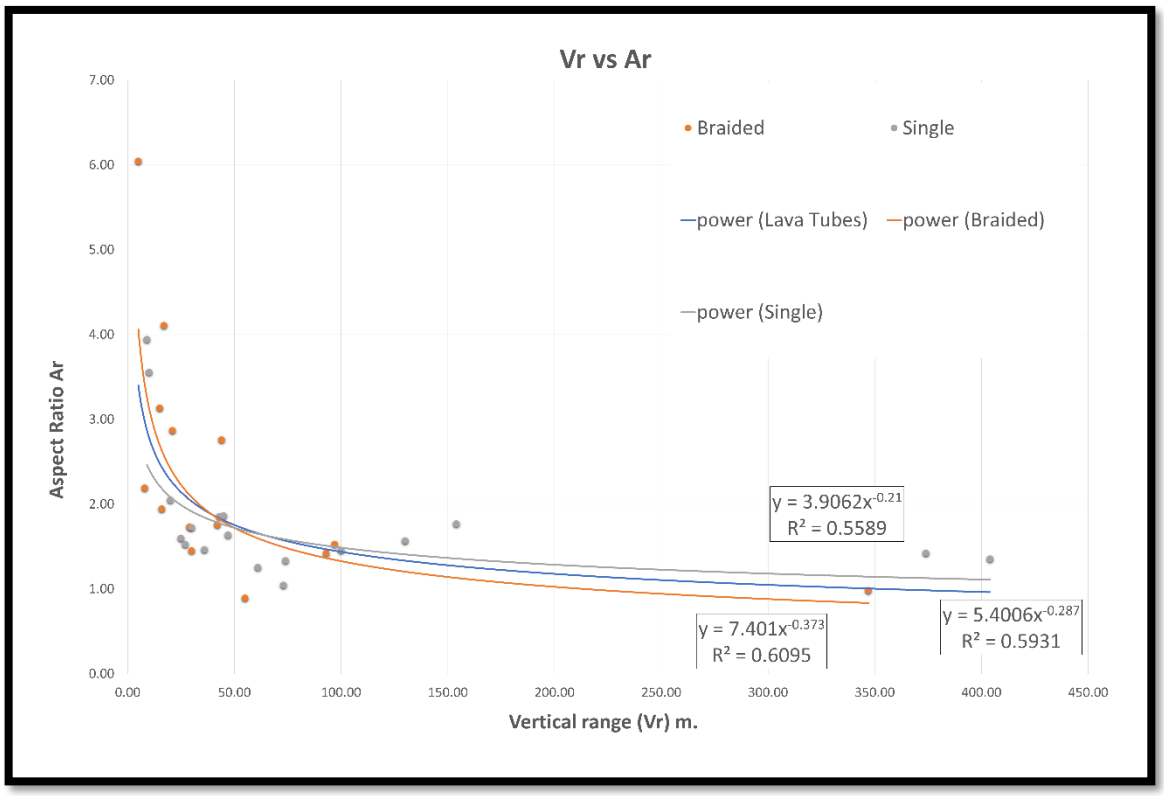

Figure 30: Vertical range (Vr) versus Aspect ratio (Ar) diagram, showing the three power fitting curves respectively related to each category: the gray line for single-type tubes, orange line for braided-type tubes, and blue line for all the data (Lava Tubes). In all of them is visible the increase of vertical range with the decrease in aspect ratio value.

6-Discussion

The comparison between plan length (**Pl)** and extension (**Es)** highlights the net subdivision between single-type and braided-type tubes (Fig. 18-19). The single-type tubes show an almost perfect linear increasing trend. In addition, with the horizontal complexity index (Hci=Pl/Es), 1.49 is the boundary between braided (above) and single-type (below). The increase of this index indicates the increase in cave complexity typical of maze caves (Fig. 18). Figure 19 shows the divergence between single and braided-types. The trend for single-type is almost perfectly linear ($R^2 = 0.9959$), while braided-type tubes are more dispersed along a different linear trend because of the development of secondary branches, which does not always lead to an increase in extension. Some lava tubes lie in the transitional range between single and braided types and have been placed in one category rather than the other based on qualitative observation. The four lava tubes in the transitional range are, *Terraced Cave* (Big Island-Hawaii), the *Tusk Cave* (Big Island-Hawaii), *Kuamo'o Point See Cave* (Big Island-Hawaii), and the *Immacolatella 1* (Mt. Etna), (Fig 31). They have an Hci really at the boundary between the two categories, (1.49 for the first two caves, 1.48 for the third, and 1,47 for the last one, see Table 8); nonetheless, secondary prominent branches are still observable placing them within the braided category. Thus, I can affirm that the morphotype of lava tubes is largely defined by the ratio between the plan map (Pl) and the extension (Es). An example is the *Salto della Giumenta* (Mt. Etna) lava tube, which shows limited loops and small secondary branches but its *Hci* index is equal to 1.04, placing it among the single tube.

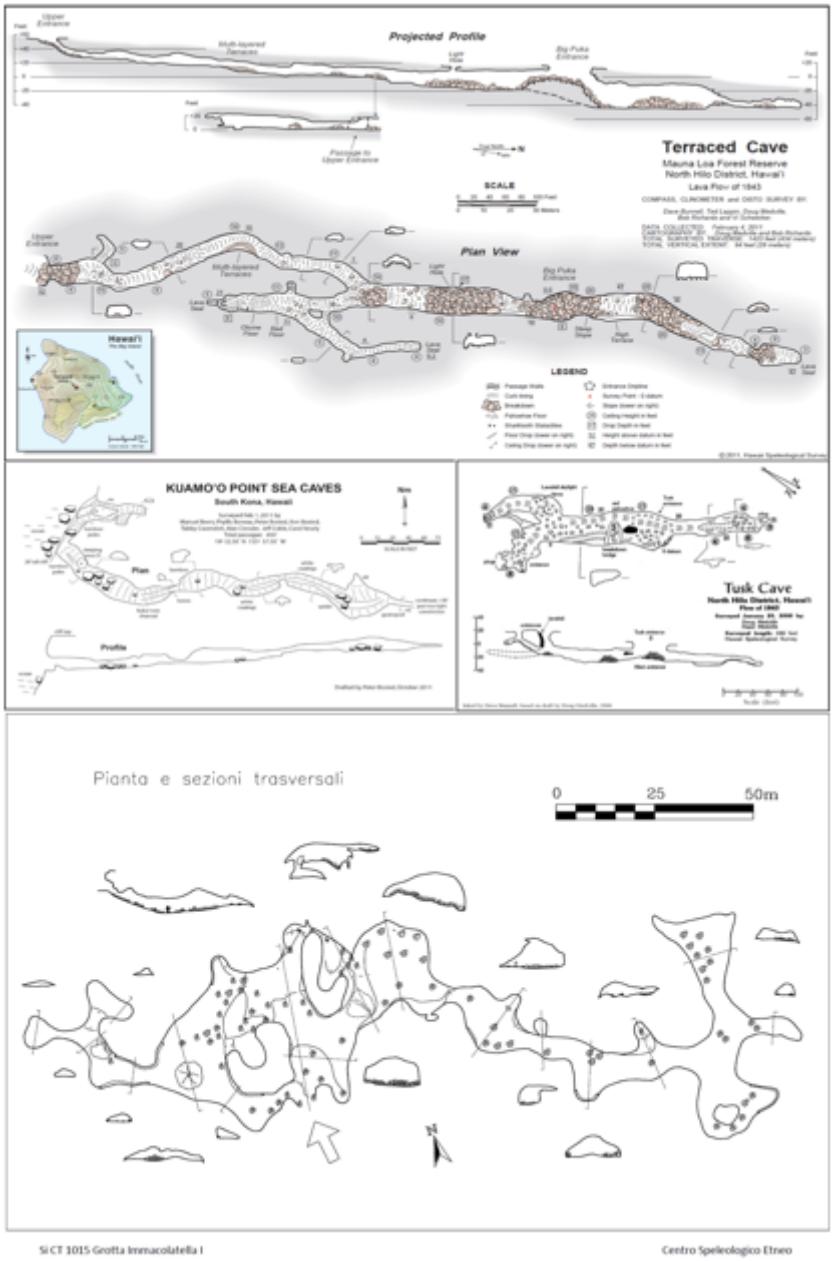

Figure 31: Hawaiian and Etna's lava tube surveys. From above: Terraced Cave and Tusk Cave (Island of Hawaii. Bunnel, 2011); Kuamo'o Point Sea Cave (Island of Hawaii. Bosted, 2011); Immacolatella Cave (Mt. Etna. Cavallaro, 1999). These lava tubes are in the transitional range between single-type and braided-type categories, showing a plan map referable to the braided-type. In addition, the ratio of the main gallery to secondary branches is low compared with lava tubes that have secondary branches but belong to the single-type category.

In addition to morphotype subdivision, an attempt was made to find a parameter that controlled the formation of different lava tube patterns. In literature, the effusion rate, time-length of eruption, and slope are suggested as fundamental parameters that can affect the lava tube patterns and dimensions. In this work I took into account the average slope of the lava tubes (detectable from the surveys) and compared it with Hci, showing no correlation with cave patterns. The only significant evidence is related to the formation of single tube which span to the 0-25° range while braided are mainly confined in the range 0-15° with only two peculiar exceptions forming over 35° (Fig. 21). Additionally, I compared also real length with the average slope of the lava tubes, but no correlation was found. Hence the slope of the lava tubes seems to have a very limited role in the general development of lava tubes, consequently, other parameters are needed such as effusion rate, vertical range, and duration of the activity.

As suggested by Wadge (1978) for the lava flow field on Mount Etna, a change in effusion rate probably increases the likelihood of new flow development. The new flow will have the potential to achieve a greater or lesser maximum distance depending on the nature of the changes of effusion rates and time length of the active phases. This may be also the reason that leads a lava tube to develop a series of side branches. The huge problem is the absence of data for the effusion rate and time-length of eruptions for the lava tubes taken into account in this work. By knowing these parameters would be possible a better understanding on their effect on the lava tube patterns.

The effusion rate is often related to the length of the lava flow (Wadge, 1978; E. Rader, et al. 2017) and the thermal efficiency of lava tubes allows to extend the length of any lava flow field (Calvari and Pinkerton, 1999; Tomasi et al., 2022). Nonetheless, the real length measured on lava tubes surveys is not the total length of the tube, due to the possibility of tube disruption, which does not allow access to other tube segments. Examples are the Tre Livelli-KTM system (Mt. Etna) and La Corona lava tube (Lanzarote-Canary Island) which have many segments interrupted by collapse or tube filling. So, it is not possible to make a direct relation between effusion rate and lava tube lengths, due to still undiscovered and not accessible tube segments. With the increase of

the effusion rate is expected an increase also in the dimension of the caves, meaning an increase of plan surface, area of the longitudinal section as well as the average linear volume of the caves. Indeed the real length (Lr) shows a good linear correlation with Ap for the single-type tubes (R^2 between 0.85 and 0.96) and, a much weaker one for the braided-type tubes (R^2 between 0.5 and 0.6).

For this reason, I related the lava tube extension to the area of the plan surface finding a good linear correlation for both the categories. Therefore, extension is the best parameter to express the length of lava tubes for each category. The outliers, found in Figure 26, are characterized by a huge plan surface against a limited extension. These results might indicate that prosecutions of lava tube conduits were not yet discovered because inaccessible. Indeed, since the extension and the area of the plan map are well correlated (R^2 always over 0.94), when Ap is unexpectedly high with respect to Es, it is most likely that the measured extension is not corresponding to the real one. A good example is the *Immacolatella 1* cave (Mt.Etna), which has a high value of Ap/Es ratio. In the present day the cave is indeed characterized by multiple collapses, instead originally, it was connected with other caves in the area *Immacolatella 2* and *3* (Cavallaro, 1999), and probably also with *Tedeschi* cave, (Mt. Etna), (Bonaccorso and Cavallaro, 1999).

The area of the plan map (Ap) may also be a consequence of several processes such as: shallow inflation, lateral erosion, or lateral coalescence, indeed the enlarged tunnel could have grown by capturing nearby conduits (Calvari and Pinkerton, 1999; Tomasi et al., 2022). Hence, the lava tubes that diverge from the exponential increasing trend, relating instead to the moderate increasing trend observed in Figure 28, may have not undergone lateral erosion or coalescence between tubes. Indeed, these tubes are characterized by several parallel tubes, which have not undergone coalescence, this implies that even if the effusion rate leads to the development of the lava tube extensions, it is not enough for the lateral coalescence processes to occur. In addition, some caves may have suffered an evolution, that led to the decrease in conduits size due to cooling and solidifying of lava along the sides and roof of the original conduits, leading to a reduction in ap without a decrease in extension. For example, lava tubes that show multi-level sections probably suffered a decrease in effusion rate, which allowed the lava to solidify as a lining wall and increase flow ledges up to their junction with the formation of a secondary ceiling as

shown by Kempe et al., 2021 for Cueva del Cascajo and; Tomasi et al., 2022 for La Corona lava tube.

Depending on the type of genetic process we expect an increase in conduit width for shallow inflation and, by contrast, an increase in conduit height due to vertical erosion for deep-inflated lava tubes. As for overcrusted tubes, neither of those cases occur, the cross-section should display a similar height and width.

The average aspect ratio (Ar) was compared with the vertical range (Vr), to understand the role of flow velocity for the genesis and morphologies of the lava tubes (Fig. 30). Indeed, considering the vertical range of the caves as the potential energy of lava flow, and, by consequence, its kinetic energy, it can be stated that with the increase of the vertical range, the average flow velocity also increases. This leads to a more erosive (even turbulent) status regime of the flow and, consequently, more effective vertical incisions of the tube floor by thermo-mechanical erosion. The final cross-section is higher than wider (indeed low aspect ratios, $Ar < 1$).

The deep-inflated lava tubes should generally have a greater vertical range due to their formation process through inflation along deep inception horizons following lava flow boundaries of pre-existing lava sequences. In addition, an increase in the width of the conduits over their highs of deep-inflated tubes is hypothesized only during their inception phase. During this phase, if the inception horizon exploited by the lava is made up of weak materials (e.g., a pyroclastic layer), it will be more easily laterally consumed by thermal erosion with respect to the erosion of its more massive roof and floor. This process has been well described by Tomasi et al., (2022), for *La Corona* lava tube in Lanzarote (Canary Islands), (Tomasi et al., 2022). After this stage, the conduit is enlarged by downward thermo-mechanical erosion and breakdown phenomena (Kempe., 2019; Sauro et al., 2020), resulting in an average aspect ratio of less than 1 ($Ar < 1$). On the other hand in shallow inflations, we expect an increase in the width of the conduits only paced by the effusion rates because these tubes are generally related to low values of vertical ranges (Vr), which does not allow the flowing magma to reach velocity enabling floor undercutting and vertical erosion as seen for the deep-inflated tubes. Thus the resulting Ar are always over 1 and more generally above 2.

The above considerations elegantly explain the diagram showing lower aspect ratio values matching the highest vertical range and *vice versa.* The tubes not strictly following this general rule and showing small aspect ratios (Ar) against a modest vertical range (Vr) can likely attributed to overcrusted type tubes that being closure of lava channels are often more isodiametric. Thus, given the good correlation between Vr and Ar, it seems unlikely that the effusion rate alone might increase the velocity of the flow up to values enabling thermo-mechanical erosion and thus decreasing of the Ar. Hence the geometry of the cross-section is a good marker of the process that led to the final morphology of the lava tubes. An elongated horizontal ellipse, probably refers to the shallow inflation process, while a triangular shape could be a consequence of the *overcrusting* process or the. The deep-inflated lava tubes are characterized by thermo-mechanical erosion of the cave floor, which means a vertically elongated development of the cross-section.

Growth of lining walls and flow ledges in shallow and deep-inflated tubes can also affect the Aspect ratio of the cave sections. These events e can create complex geometries, explainable through the evolution and changes in the effusion rate, as well as the duration of the eruption. If the effusion is long-standing and with a stable or slowly decreasing effusion rate, we will observe a growth of lining wall and flow ledges with the eventual formation of multi-level tubes. In case of deep-inflated tube the vertical elongated aspect ratio of the tube can be transformed into more enlarged tube sections if the single tubes of the multilevel system are considered. In the case of shallow inflation, the same condition would cause a decrease of the tube section, by reducing the aspect ratio (Ar) value.

Even comparing the average aspect ratio with the Ap/Es ratio (Fig. 29) it is possible to discriminate overcrusting, deep, and shallow inflated tubes as well as their evolution. : Ar ranging from 2 to 1, associated with low values of Ap/Es might indicate “overcrusting” process. But suppose these values of Ar are associated with a high value of Ap/Es, related to high values of the effusion rate. In that case, this might mean that the lava tubes are deep-inflated (La Corona, Lanzarote), instead high values of Ar (Ar > 2) often related to a high value of Ap/Es, are typical of the lava tubes that form by shallow inflation process due to their lower velocities and erosive power (due to less vertical range) compared to the deep-inflated. Naturalistas (Lanzarote-Canary Island) cave is a good example of this case (Fig. 29). Finally if the Ar is about or less than 1 the lava tube had probably suffered

a vertical incision, this is the case of Cueva di Elena (Santa Cruz Island, Galapagos). The latter case could be related to deep-inflation.

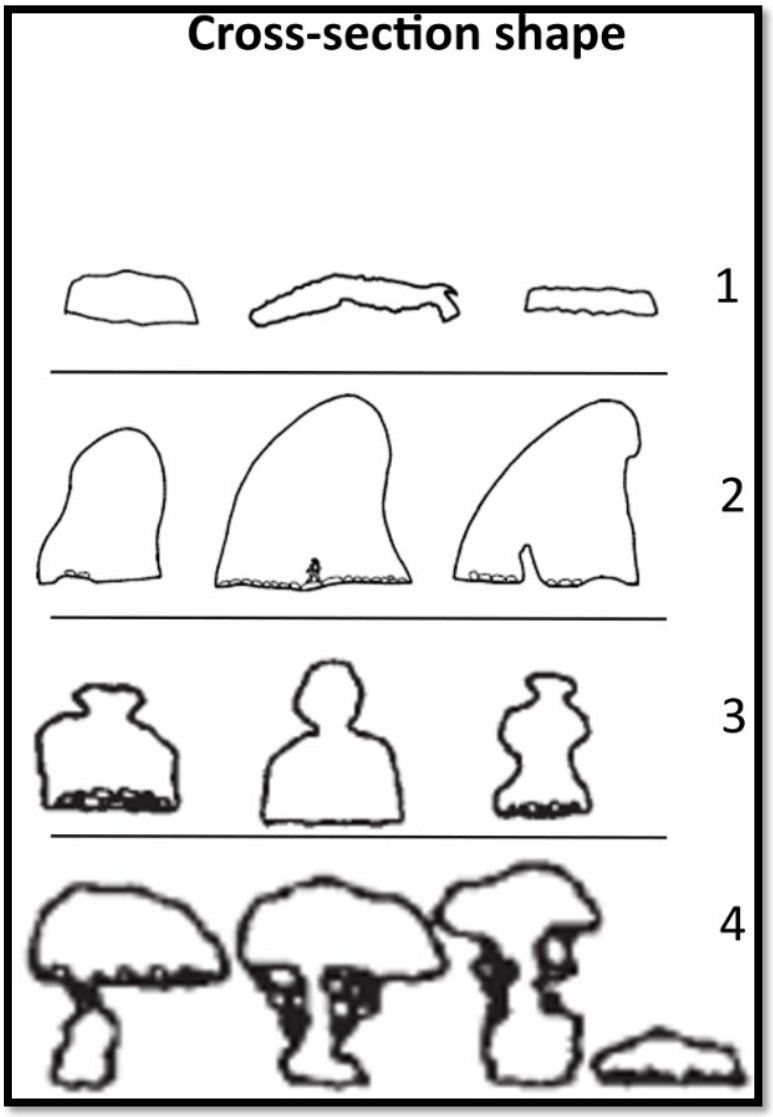

Figure 32: Possible evolution of cross-section geometries, seen in four different lava tubes. 1) Tedeschi cave (Mt. Etna) cross-section, an example of elongated ellipse; 2) Catanese 1 (Mt. Etna) Cave cross-section, triangular shape, may be due to growth of lining walls; 3) Kastdalen Cave (Santa Cruz Island-Galapagos) cross-section, more complex geometries, explainable by the growth of flow ledges; 4) Elena's cave (Santa Cruz Island-Galapagos) cross-section, closure of the flow ledges or incision of the cave floor by thermo-mechanical erosion.

7-Conclusion

Through the digitalization of lava tube surveys and morphometric analysis I have extracted 27 parameters, most of them not reported in survey inventories. This allowed me to perform more detailed description of these subsurface structures, and their related processes and evolutions.

The ratio between Plan length (Pl) and Extension (Es) (Horizontal Complexity index Hci) describes how much lava tubes are characterized by braided patterns, allowing the subdivision of the lava tubes into two main morphotypes, single-type and braided-type. I have also carried out some comparisons between slope and other parameters to better understand the role of slope in the evolution of lava tube morphologies and dimensions. In particular, the slope was compared with the Horizontal complexity index (Hci) and real length (Lr), showing how it does not affect the lava tube morphotype and development. For this reason, I tried to figure out the role of effusion rate and duration of the eruption in lava tube formations. Parameters such as the real length (Lr), plan length (Pl), extension (Es), area of plan map (Ap), area of longitudinal section (As), and average linear volume (aLV), quantitatively describe the size of the lava tubes examined. The relationship between the above mentioned parameters can give an idea of the effusion rate and of the time-length eruption, which are often related to the length of the lava tubes and their size (Chapters 1–3).

In particular, the relationship between the Extension and Plan map area, are controlled by effusion rate and the duration of the eruption since they are not dependent on morphotypes (single and braided) Indeed, for high values of Es and Ap, it is expected a high effusion rate, maintained stable for a long period. In contrast, the high value of the Es with a low value of the Ap is probably related to a first high effusion rate, which allows to increase in the extension of the tube, followed by a decrease in effusion rate, which remains stable for a long time, can lead to the growth of lining walls and so the decrease of Ap.

The velocity of the flow is c controlled by the vertical range, which evidently affects the erosive power of the flow. In Figure 30, is clear how this parameter (Vr) affects the average aspect ratio of the lava tube cross-sections. Indeed, the increase in vertical range (Vr) involves a decrease in the average aspect ratio (Ar). Furthermore, in some cases, changes in effusion rate can lead to a decrease in the aspect ratio due to lining wall and

flow ledges growth, so low values of the average aspect ratio (Ar) can be observed even with low values of the vertical range (Vr). Moreover, low values of Ar and Vr are possible also due to the overcrusting process.

This first work opens several possibilities in lava tube studies, which can be substantially improved thanks to the huge amount of surveys reported in cave inventories throughout the world. This would increase the dataset here taken into consideration and improve the statistical analysis here reported. The understanding of the processes of inception and evolution of lava tubes on the Earth might help in discovering what lies beneath the surface even of other planets, and help in preparing future underground explorations.

Reference

Acocella, V., & Neri, M. (2005). Structural features of an active strike-slip fault on the sliding flank of Mt. Etna (Italy). *Journal of Structural Geology*, *27*(2), 343-355.

Allred, K., & Allred, C. (1997). Development and morphology of Kazumura cave, Hawaii. *Journal of Caves and Karst Studies*, *59*, 67-80.

Bailey, J. E., Harris, A. J., Dehn, J., Calvari, S., & Rowland, S. K. (2006). The changing morphology of an open lava channel on Mt. Etna. *Bulletin of volcanology*, *68*, 497-515.

Bargar, K. E., & Jackson, E. D. (1974). Calculated volumes of individual shield volcanoes along the Hawaiian-Emperor chain. *J. Res. US Geol. Surv*, *2*(5), 545-550.

Barreca, G., Corradino, M., Monaco, C., & Pepe, F. (2018). Active tectonics along the south east offshore margin of Mt. Etna: New insights from high-resolution seismic profiles. *Geosciences*, *8*(2), 62.

Branca, S., Coltelli, M., Groppelli, G., & Lentini, F. (2011). Geological map of Etna volcano, 1: 50,000 scale. *Italian Journal of Geosciences*, *130*(3), 265-291.

Branca, S., & Ferrara, V. (2013). The morphostructural setting of Mount Etna sedimentary basement (Italy): Implications for the geometry and volume of the volcano and its flank instability. *Tectonophysics*, *586*, 46-64.

Bonaccorso, R., Santi, G., (1999). La Grotta di Nuovalucello 1. In: *DENTRO IL VULCANO: IL LIBRO Le Grotte dell'Etna Catania*: Centro Speleologico Etneo - Parco dell'Etna. 174-175.

Bonaccorso, R., Cavallaro, F., (1999). La Grotta dei Tedeschi. In: *DENTRO IL VULCANO: IL LIBRO Le Grotte dell'Etna Catania*: Centro Speleologico Etneo - Parco dell'Etna. 190-191.

Bonaccorso, R., Santi, G., (1999). La Grotta degli Archi. In: *DENTRO IL VULCANO: IL LIBRO Le Grotte dell'Etna Catania*: Centro Speleologico Etneo - Parco dell'Etna. 225-227.

Bonaccorso, R., Santi, G., (1999). La Grotta del Santo. In: *DENTRO IL VULCANO: IL LIBRO Le Grotte dell'Etna Catania*: Centro Speleologico Etneo - Parco dell'Etna. 230-233

Bonaccorso, R., Santi, G., (1999). La Grotta del Gelo. In: *DENTRO IL VULCANO: IL LIBRO Le Grotte dell'Etna Catania*: Centro Speleologico Etneo - Parco dell'Etna. 252-254.

Bonaccorso, R., Marino, A., Santi, G., (1999). La Grotta del Salto della Giumenta. In: *DENTRO IL VULCANO: IL LIBRO Le Grotte dell'Etna Catania*: Centro Speleologico Etneo - Parco dell'Etna. 315-317.

Bosted, A., & Bosted, P., (2009). Exploration of Manu Nui Lava Tube Hawai'i Speleological Survey Newsletter – National Speleological Society. 3-13

Bosted, A., (2011). Kuamo'o Point Sea Cave. Hawai'i Speleological Survey Newsletter - National Speleological Society. 32-35.

Bunnell, D. (2008). *Caves of Fire: Inside America's Lava Tubes*. National Speleological Society.

Bunnel, D., (2010). The Exploration and Survey of Oozing Red Cave System. Hawai'i Speleological Survey Newsletter - National Speleological Society. 3-17

Bunnel, D., (2011). The 2011 HSS Expedition: Caves of the Lower 1843 Flow. Hawai'i Speleological Survey Newsletter - National Speleological Society. 3-13.

Calvari, S., & Pinkerton, H. (1999). Lava tube morphology on Etna and evidence for lava flow emplacement mechanisms. *Journal of Volcanology and Geothermal Research*, *90*(3-4), 263-280.

Carracedo, J. C., Day, S., Guillou, H., Badiola, E. R., Cañas, J. A., & Torrado, F. P. (1998). Hotspot volcanism close to a passive continental margin: the Canary Islands. *Geological magazine*, *135*(5), 591-604.

Carracedo, J. C., & Perez-Torrado, F. J. (2013). Geological and Geodynamic context of the Teide Volcanic complex. In *Teide Volcano: Geology and Eruptions of a Highly Differentiated Oceanic Stratovolcano* (pp. 23-36). Berlin, Heidelberg: Springer Berlin Heidelberg.

Cavallaro, F., (1999). Grotta Micio Conti. In: *DENTRO IL VULCANO: IL LIBRO Le Grotte dell'Etna Catania*: Centro Speleologico Etneo - Parco dell'Etna. 186-187.

Cavallaro, F., (1999). Grotta Immacolatella 1. In: *DENTRO IL VULCANO: IL LIBRO Le Grotte dell'Etna Catania*: Centro Speleologico Etneo - Parco dell'Etna. 192-193.

Cavallaro, F., (1999). La Grotta della Catanese 1. In: *DENTRO IL VULCANO: IL LIBRO Le Grotte dell'Etna Catania*: Centro Speleologico Etneo - Parco dell'Etna. 220-221.

Celli, N. L., Lebedev, S., Schaeffer, A. J., & Gaina, C. (2021). The tilted Iceland Plume and its effect on the North Atlantic evolution and magmatism. *Earth and Planetary Science Letters*, *569*, 117048.

Clague, D. A., & Dalrymple, G. B. (1987). The Hawaiian-emperor volcanic chain. *US Geol. Surv. Prof. Pap*, *1350*, 5-54.

Coello, J., Cantagrel, J. M., Hernán, F., Fúster, J. M., Ibarrola, E., Ancochea, E., ... & Cendrero, A. (1992). Evolution of the eastern volcanic ridge of the Canary Islands based on new K Ar data. *Journal of Volcanology and Geothermal Research*, *53*(1-4), 251-274.

Dauteuil, O., & Bergerat, F. (2005). Interactions between magmatism and tectonics in Iceland: a review. *Geodinamica acta*, *18*(1), 1-9.

Davis, N. W., (2009). Tom's Hole. Caving on the Lower 1855 Flow. Hawai'i Speleological Survey Newsletter - National Speleological Society. 14.

De Beni, E., Branca, S., Coltelli, M., Groppelli, G., & Wijbrans, J. R. (2011). 40Ar/39Ar isotopic dating of Etna volcanic succession. *Italian Journal of Geosciences*, *130*(3), 292-305.

Dragoni, M., Piombo, A., & Tallarico, A. (1995). A model for the formation of lava tubes by roofing over a channel. *Journal of Geophysical Research: Solid Earth*, *100*(B5), 8435-8447.

Eiríksson, J., & Símonarson, L. A. (2021). A brief Résumé of the geology of Iceland. *Pacific-Atlantic Mollusc Migration: Pliocene Inter-Ocean Gateway Archives on Tjörnes, North Iceland*, 1-11.

Fagents, S. A., & Greeley, R. (2001). Factors influencing lava-substrate heat transfer and implications for thermomechanical erosion. *Bulletin of Volcanology*, *62*, 519-532.

Fletcher, C. H., Bochicchio, C., Conger, C. L., Engels, M. S., Feirstein, E. J., Frazer, N., ... & Vitousek, S. (2008). Geology of Hawaii reefs. *Coral Reefs of the USA*, 435-487.

Francis, P. (1993). *Volcanoes. A planetary perspective*.

Gallardo, G., & Toulkeridis, T. (2008). Volcanic Caves and Other Speleological Attractions. Santa Cruz, Galápagos.

Giudice, G., Santi, G., (1999). La Grotta del Burrò. In: *DENTRO IL VULCANO: IL LIBRO Le Grotte dell'Etna Catania*: Centro Speleologico Etneo - Parco dell'Etna. 246-247.

Giudice, G., Santi, G., (1999). La Grotta del Diavolo. In *DENTRO IL VULCANO: IL LIBRO Le Grotte dell'Etna Catania*: Centro Speleologico Etneo - Parco dell'Etna. 248-249.

Giudice, G., Leotta, A., Santi, G., (1999). La Grotta Cutrona. In: *DENTRO IL VULCANO: IL LIBRO Le Grotte dell'Etna Catania*: Centro Speleologico Etneo - Parco dell'Etna. 304-308.

Greeley, R., Fagents, S. A., Harris, R. S., Kadel, S. D., Williams, D. A., & Guest, J. E. (1998). Erosion by flowing lava: Field evidence. *Journal of Geophysical Research: Solid Earth*, *103*(B11), 27325-27345.

Grímsson, F., Denk, T., & Símonarson, L. A. (2007). Middle Miocene floras of Iceland—the early colonization of an island?. *Review of Palaeobotany and Palynology*, *144*(3-4), 181-219.

Halliday, W., 2004. Volcanic caves. Encyclopedia of Caves and Karst Science. 760. Fitzroy Dearborn, New York, pp. 764.

Hansen Machín, A. R., & Pérez Torrado, F. (2005). The island and its territory: volcanism in Lanzarote.

Hernández, J. J., Izquierdo, I., & Oromi, P. (1991, August). Contribution to the vulcanospeleology of the Galapagos Islands. In Procedings of the 6th intenational symposium on vulcanospeleology Hawaii Islands (pp. 204-220).

Hoernle, K. A. J., & Carracedo, J. C. (2009). Canary Islands geology. University of California Press.

Hróarsson, B. (2006). Íslenskir hellar. Vaka-Helgafell.

Jones, M. P., Soule, S. A., Gonnermann, H. M., Le Roux, V., & Clague, D. A. (2018). Magma ascent and lava flow emplacement rates during the 2011 Axial Seamount eruption based on CO2 degassing. *Earth and Planetary Science Letters*, *494*, 32-41.

Kempe, S., & Henschel, H. V., (2008). Thurston Lava Cave, the Most Visited Tube in the World. What Do We Know about It? Hawai'i Speleological Survey Newsletter - National Speleological Society. 16-24.

Kempe, S., Bauer, I., Bosted, P., Coons, D., & Elhard, R. (2010, August). Inflationary versus crusted-over roofs of pyroducts (lava tunnels). In *Proceedings 14th International Symposium on Vulcanospeleology* (Vol. 93).

Kempe, S. (2019). Volcanic rock caves. In *Encyclopedia of caves* (pp. 1118-1127). Academic Press.

Kempe, S., Middleton, G., Addison, A., Toulkeridis, T., & Hoese, G. (2021). NEW INSIGHTS INTO THE GENESIS OF PYRODUCTS OF THE GALÁPAGOS ISLANDS, ECUADOR. *Acta Carsologica*, *50*(1).

Klimchouk, A.B., 2003: Cave morphometry.- In: Gunn, J. (ed.) Encyclopedia of cave and karst science, Fitzroy Dearborn, pp. 1120-1125, New York.

Langenheim, V. A., & Clague, D. A. (1987). The Hawaiian-Emperor volcanic chain. *Part*, *2*, 55-84.

Licitra, G. M., Santi, G., (1999). La Grotta di Monte Intraleo. In: *DENTRO IL VULCANO: IL LIBRO Le Grotte dell'Etna Catania*: Centro Speleologico Etneo - Parco dell'Etna. 234-236.

Marino, A., Santi, G., (1999). La Grotta Corsaro. In: *DENTRO IL VULCANO: IL LIBRO Le Grotte dell'Etna Catania*: Centro Speleologico Etneo - Parco dell'Etna. 215-216.

Marino, A., Santi, G., (1999). La Grotta MA.RA.SCA. In: *DENTRO IL VULCANO: IL LIBRO Le Grotte dell'Etna Catania*: Centro Speleologico Etneo - Parco dell'Etna. 297-298.

Mcdonald, G. A., Abbott, A., & Peterson, F. L. (1983). *Volcanoes in the sea: the geology of Hawaii*. University of Hawaii Press.

Medville, D., (2009). Caving on the Lower 1855 Flow. Hawai'i Speleological Survey Newsletter - National Speleological Society. 3-7

Peterson, D. W., & Swanson, D. A. (1974). Observed formation of lava tubes during 1970–71 at Kilauea Volcano, Hawaii. *Studies in Speleology*, *2*(6), 209-222.

Peterson, D. W., & Moore, R. B. (1987). Geologic history and evolution of geologic concepts. In *Island of Hawaii* (Vol. 1350, pp. 149-189).

Peterson, D. W., Holcomb, R. T., Tilling, R. I., & Christiansen, R. L. (1994). Development of lava tubes in the light of observations at Mauna Ulu, Kilauea Volcano, Hawaii. *Bulletin of Volcanology*, *56*, 343-360.

Piccini, L. (2011). Recent developments on morphometric analysis of karst caves. *Acta Carsologica*, *40*(1).

Rader, E., Vanderkluysen, L., & Clarke, A. (2017). The role of unsteady effusion rates on inflation in long-lived lava flow fields. *Earth and Planetary Science Letters*, *477*, 73-83.

Richards, B., & Szukalski, B., (2010). Survey of Hana Gardenland Cave and Nahiku Road Caves. Hawai'i Speleological Survey Newsletter - National Speleological Society. 10-15.

Romero, J. V., & Galindo, I. (2019). Geological and Geographical Setting of Lanzarote and Global Geopark. *Lanzarote and Chinijo Islands Geopark: From Earth to Space*, 19.

Santagata, T., Sauro, F., Massironi, M., Pozzobon, R., Del Vecchio, U., Lazzaroni, M., ... & Mateo Medero, E. (2018, April). Subsurface laser scanning and photogrammetry in the Corona lava tube system, Lanzarote, Spain. In *EGU General Assembly Conference Abstracts* (p. 5290).

Santi G. (1999). La Grotta dei Lamponi. In: *DENTRO IL VULCANO: IL LIBRO Le Grotte dell'Etna Catania*: Centro Speleologico Etneo - Parco dell'Etna. 261-263.

Santi, G. (1999). La Grotta dei Tre Livelli. In: *DENTRO IL VULCANO: IL LIBRO Le Grotte dell'Etna Catania*: Centro Speleologico Etneo - Parco dell'Etna. 286-289.

Santi G. (1999). La Grotta KTM. In *DENTRO IL VULCANO: IL LIBRO Le Grotte dell'Etna Catania*: Centro Speleologico Etneo - Parco dell'Etna. 290-291.

Sauro, F., Pozzobon, R., Santagata, T., Tomasi, I., Tonello, M., Martínez-Frías, J., ... & Massironi, M. (2019). Volcanic caves of Lanzarote: A natural laboratory for understanding volcano-speleogenetic processes and planetary caves. *Lanzarote and chinijo islands geopark: From earth to space*, 125-142.

Sauro, F., Pozzobon, R., Massironi, M., De Berardinis, P., Santagata, T., & De Waele, J. (2020). Lava tubes on Earth, Moon and Mars: A review on their size and morphology revealed by comparative planetology. *Earth-Science Reviews*, *209*, 103288.

Schiano, P., Clocchiatti, R., Ottolini, L., & Busa, T. (2001). Transition of Mount Etna lavas from a mantle-plume to an island-arc magmatic source. *Nature*, *412*(6850), 900-904.

Sherrod, D. R., Sinton, J. M., Watkins, S. E., & Brunt, K. M. (2021). *Geologic map of the State of Hawaii* (No. 3143). US Geological Survey.

Storey, M., Duncan, R. A., & Tegner, C. (2007). Timing and duration of volcanism in the North Atlantic Igneous Province: Implications for geodynamics and links to the Iceland hotspot. *Chemical Geology*, *241*(3-4), 264-281.

Thordarson, T., & Larsen, G. (2007). Volcanism in Iceland in historical time: Volcano types, eruption styles and eruptive history. *Journal of Geodynamics*, *43*(1), 118-152.

Tomasi, I., Massironi, M., Meyzen, C. M., Pozzobon, R., Sauro, F., Penasa, L., ... & Martinez-Frìas, J. (2022). Inception and evolution of La Corona Lava Tube System (Lanzarote, Canary Islands, Spain). *Journal of Geophysical Research: Solid Earth*, *127*(6), e2022JB024056.

Tonello, M. (2017). Origin and evolution of an inflated lava tube between the Mio-Pliocene volcanic complex of Famara and the Quaternary lava flows of La Corona in Lanzarote.

Van den Bogaard, P. (2013). The origin of the Canary Island Seamount Province-New ages of old seamounts. *Scientific reports*, *3*(1), 2107.

Wadge, G. (1978). Effusion rate and the shape of aa lava flow-fields on Mount Etna. *Geology*, *6*(8), 503-506

Werner, R., Hoernle, K., Barckhausen, U., & Hauff, F. (2003). Geodynamic evolution of the Galápagos hot spot system (Central East Pacific) over the past 20 my: Constraints from morphology, geochemistry, and magnetic anomalies. *Geochemistry, Geophysics, Geosystems*, *4*(12).

White, W. M., McBirney, A. R., & Duncan, R. A. (1993). Petrology and geochemistry of the Galápagos Islands: Portrait of a pathological mantle plume. *Journal of Geophysical Research: Solid Earth*, *98*(B11), 19533-19563.

Wilson, J. T. (1963). A possible origin of the Hawaiian Islands. *Canadian Journal of Physics*, *41*(6), 863-870.

Wilson, D. S., & Hey, R. N. (1995). History of rift propagation and magnetization intensity for the Cocos-Nazca spreading Center. *Journal of Geophysical Research: Solid Earth*, *100*(B6), 10041-10056.